

Colloquium: Electronic instabilities in self-assembled atom wires

Paul C. Snijders*

Materials Science and Technology Division, Oak Ridge National Laboratory, Oak Ridge, Tennessee 37831, USA

Hanno H. Weitering

Department of Physics and Astronomy, The University of Tennessee, Knoxville, Tennessee 37996, USA
and Materials Science and Technology Division, Oak Ridge National Laboratory, Oak Ridge, Tennessee 37831, USA

(Published 12 February 2010)

Many quasi-one-dimensional (1D) materials are experimental approximations to the textbook models of Peierls instabilities and collective excitations in 1D electronic systems. The recently observed self-assembly of atom wires on solid surfaces has provided fascinating new insights into the nature of their structural and electronic instabilities, from both real-space and momentum-space perspectives. In this Colloquium, three of the most studied atom wire arrays are highlighted, all featuring multiple surface-state bands. One of these is made of indium atoms on a flat silicon (111) surface, while the two others consist of gold atoms on surfaces that are vicinal to Si(111). The experimental and theoretical results are discussed with a focus on the detailed mechanisms of the observed phase transitions and on the role of microscopic defects.

DOI: [10.1103/RevModPhys.82.307](https://doi.org/10.1103/RevModPhys.82.307)

PACS number(s): 71.30.+h, 71.45.Lr, 73.20.-r, 73.22.Gk

CONTENTS

I. Introduction	307
A. Charge-density waves	308
II. Gold-Induced Quasi-One-Dimensional Atom Wires on Silicon Surfaces	309
A. Au/Si(111)	309
B. Au/Si(557)	310
1. Atomic and electronic structure	310
2. Metal-insulator transition	311
3. Alternative model of the transition	312
C. Au/Si(553)	314
1. Atomic and electronic structure	314
2. Metal-insulator transitions in multiple bands	316
3. The doublet of half-filled bands	318
4. Defects and interchain correlations	319
III. In Atom Wires on Si(111)	321
A. In/Si(111)	321
1. Atomic and electronic structure	321
2. Metal-insulator transition	322
3. Order-parameter fluctuations	322
4. Alternative model of the transition	324
5. Possible evidence of non-Fermi-liquid behavior	326
6. Role of defects	326
IV. Concluding Remarks	327
Acknowledgments	327
References	327

I. INTRODUCTION

One-dimensional (1D) conductors have always captured the imagination of physicists. While a strictly 1D material largely remains a theoretical construct, a vast number of materials can be viewed as quasi-1D, making them interesting test cases for theoretical predictions and for learning the fundamentals of electronic transport in extreme low-dimensional material systems and devices created via nanotechnology. In 1955, Peierls analyzed a chain of atoms with a single orbital basis and concluded that such a chain cannot be metallic (Peierls, 1955). The general principle is shown in Fig. 1. In this textbook example, each atomic orbital contains one valence electron so the associated energy band is half

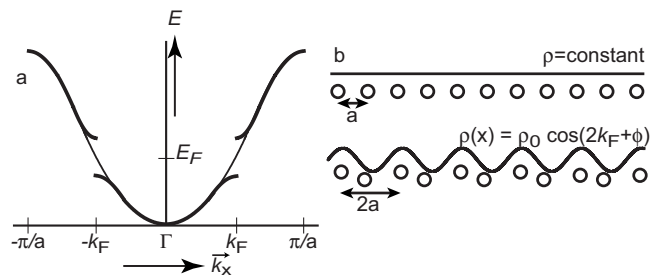


FIG. 1. The effect of a Peierls distortion on (a) a half-filled 1D band structure and (b) the charge density and the atomic structure. In (a) the thin continuous band belongs to the undistorted metal and the bold printed gapped band belongs to the Peierls distorted system. (b) The periodic modulation of the charge density and the period doubling of the lattice structure are shown.

*snijderspc@ornl.gov

filled. Peierls pointed out that a period-doubling lattice distortion would create a Brillouin-zone boundary right at the k point indicated by the Fermi wave vector and, consequently, a gap opens up at the Fermi energy (E_F). The electronic energy gain associated with the gap creation scales as $u^2 \ln u$, where u is the amplitude of the periodic lattice distortion. The penalty for the distortion is proportional to u^2 so the total energy minimizes at nonzero distortion (Grüner, 1988). This principle can easily be generalized. For a band filling of $1/n$, the Peierls instability opens up a gap at wave vector $k_F = \pi/na$, and the new periodicity $\lambda = \pi/k_F = na$ (where a is the lattice parameter of the metallic phase) is not necessarily commensurate with the lattice.

The Luttinger liquid model provides a sharply contrasting picture of a 1D electron system [for a review, see Voit (1995)]. Whereas the Peierls theorem is based on a single electron Bloch formalism, the Luttinger liquid model emphasizes strong correlations. In fact, it only defines collective excitations in which charge-density excitations and spin-density excitations propagate with different group velocities, a phenomenon known as spin-charge separation. The concept of a quasiparticle carrying both spin and charge has no meaning in the Luttinger liquid. The Luttinger liquid and Peierls condensate are mutually exclusive in that a Peierls distortion preempts the formation of a Luttinger liquid because the Peierls gap is generally larger than the energy scale of Luttinger liquid physics. Conversely, in a Luttinger liquid the density of states (DOS) at the Fermi level is strongly reduced due to strong interactions. Because the single-particle concept is meaningless in a Luttinger liquid, the Peierls argument is not applicable.

The atom wire arrays in this Colloquium all exhibit electronic instabilities that are reminiscent of a Peierls instability. They are generally referred to as charge-density wave (CDW) instabilities. These instabilities likely eradicate the possibility of observing a Luttinger liquid at low temperature. However, the (presumed) CDW instabilities are also more complex than the simple Peierls picture would suggest. They generally involve not just one but several electronic bands with significant interwire coupling. They are also coupled elastically to the substrate. Finally, even though the Peierls picture emphasizes the coupling between the electronic subsystem and atomic coordinates (i.e., electron-phonon coupling), electron correlations, magnetic interactions, spin-orbit coupling, and charged defects may all play an important role.

It appears that the quasiparticle concept still applies and thus a microscopic understanding of the symmetry-breaking principles naturally begins with a study of the Fermi contour of the high-symmetry phase. This, however, does not imply that the instabilities are entirely electronic. The total energy argument used by Peierls explains *why* a 1D crystal should spontaneously reduce its translational symmetry but it does not elucidate *how* the distortion physically occurs. It is doubtful whether one can separate the electronic instability from a lattice

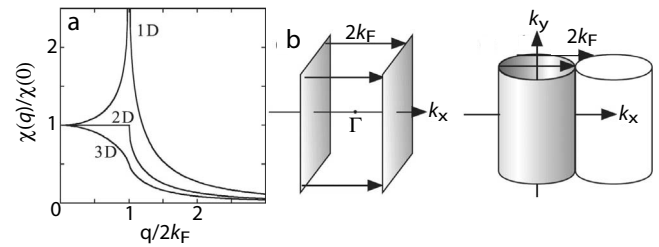


FIG. 2. Nesting and dielectric response of free electron gases. (a) Lindhard response function for a free-electron gas in one, two, and three dimensions. (b) Fermi surface nesting for a free-electron gas in one and two dimensions. From Aruga, 2002.

instability as they always occur simultaneously (Johannes and Mazin, 2008).

A. Charge-density waves

The role of the Fermi surface in a Peierls or CDW instability is best illustrated using the Lindhard dielectric susceptibility for the screening response of a free-electron gas (Aruga, 2002). When a homogeneous electron gas is subject to a static perturbation or “external” potential of wave vector q , then within linear response theory the induced charge density $\rho^{\text{ind}}(q)$ will be given by $\rho^{\text{ind}}(q) = \chi(q)V(q)$, where $V(q)$ is the q th Fourier component of the external perturbation $V(r)$ and $\chi(q)$ is the static dielectric susceptibility or “response function.” $\chi(q)$ is given by

$$\chi(q) = \frac{e^2}{q^2} \sum \frac{f(E_k) - f(E_{k+q})}{E_k - E_{k+q}}, \quad (1)$$

where the sum is over all wave vectors k . $f(E)$ is the Fermi-Dirac distribution and E_k is the energy of an electron with wave vector k . We only consider k vectors where the state $E(k)$ is occupied and $E(k+q)$ is empty, or vice versa. When $q = 2k_F$, all states within the Fermi sphere contribute to the summation. Equation (1) signals the possibility of a singularity: when the wave vector q spans the Fermi surface, the denominator vanishes. For a spherical or cylindrical Fermi surface, such singularities are inconsequential because relatively few k -point pairs contribute to the divergence. However, for nonspherical Fermi surfaces and, in particular, for Fermi surfaces with parallel (or nested) segments, there can be many k -point pairs producing a vanishing denominator (see Fig. 2). The Fermi surface of a 1D solid is perfectly nested and, consequently, the divergence at $q = 2k_F$ becomes rigorous. Any perturbation that can supply a momentum of $q = 2k_F$ will be perfectly screened. If this momentum is supplied by a phonon, then the corresponding phonon excitation will be perfectly screened, meaning that its frequency would go to zero. One thus recovers the periodic lattice distortion envisioned by Peierls. CDWs can in principle occur in higher

dimensions but the nested portion of the Fermi surface will be significantly reduced and the singularity will be much weaker.

The temperature below which the system condenses into a CDW state can be estimated from mean-field theory (Grüner, 1994). When the CDW gap is small, say ≤ 100 meV, the CDW transition temperature T_c is related to the electron-phonon coupling constant via the BCS gap equation, first derived within the context of superconductivity (Kuper, 1955; Bardeen *et al.*, 1957). This situation is usually referred to as the weak-coupling regime. Strictly speaking, mean-field theory must fail in one dimension because it ignores thermal fluctuations. Fluctuations inhibit long-range ordering at finite temperatures (Mermin and Wagner, 1966). Paradoxically, interchain coupling is thus essential for observing a Peierls phase transition, although T_c will be far below the mean-field estimate due to these fluctuations (Lee *et al.*, 1973). Strong interchain coupling could reduce T_c to zero because the nested portions of the Fermi surface disappear.

In the strong electron-phonon coupling limit, mean-field theory no longer provides an adequate description of the thermodynamic properties and the system exhibits mesoscopic fluctuations starting well below the mean-field transition temperature. To capture these fluctuations, the order parameter must be written as $|\Delta(r)| \exp[i\phi(r)]$, where $|\Delta(r)|$ and $\phi(r)$ are the temperature-dependent amplitude and phase of the order parameter.

Transitions that are driven by a soft phonon are often termed “displacive.” In such cases, the amplitude of the distortion and the energy gap constitute proper order parameters and typically follow the weak-coupling behavior. The spatial coherence of the CDW state is long. In the strong-coupling limit, the phase transition is of the order-disorder type where atoms fluctuate between different potential minima above T_c . These transitions are not necessarily associated with a soft phonon but they can involve a “soft diffusive mode,” which is equivalent to large amplitude thermal hopping between potential wells. The spatial coherence is short due to strong phase fluctuations. However, this distinction between a displacive and order-disorder transition is quite artificial and only describes the extreme cases. In many cases, CDW systems exhibit a combination of weak-coupling and strong-coupling features (Aruga, 2006). For instance, Sn on Ge(111) is considered a strong-coupling surface CDW system, which exhibits a soft phonon but no nesting (Avila *et al.*, 1999; Pérez *et al.*, 2001). Alternatively, systems with strong nesting do not always undergo a CDW transition. In fact, it has been pointed out that the nesting argument may not have any predictive power regarding the possible occurrence of a CDW (Johannes and Mazin, 2008).

Defects also play a profound role. Charged impurities can affect both amplitude and phase of the order parameter near the impurity sites and may prohibit long-range ordering (Grüner and Zettl, 1985). Theoretical studies indicated that long-range order can be completely de-

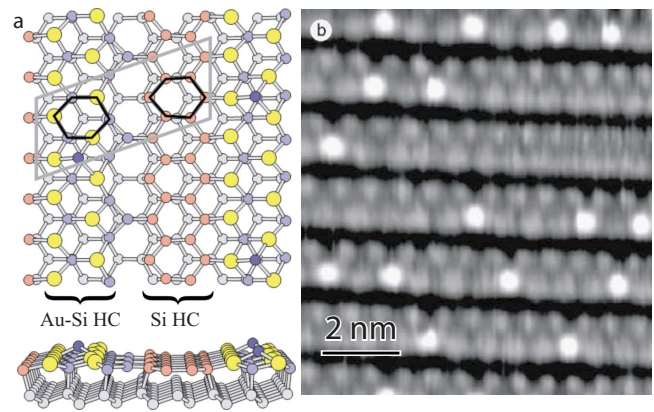


FIG. 3. (Color online) The Si(111)- 5×2 -Au reconstruction. (a) Structural model for Si(111)- 5×2 -Au. Large, light circles are Au atoms, dark circles are Si adatoms. A 5×2 unit cell and a Si (and a mixed additional Au-Si) honeycomb are indicated. (b) STM image (-1.5 V, 200 pA) of the Si(111)- 5×2 -Au wire reconstruction with Si adatoms visible as dots. From Erwin, 2003 and Kirakosian *et al.*, 2003.

stroyed by a “random external field,” meaning static or quenched disorder, if the dimensionality of the system is 2 or lower. Alternatively, defects can also act as nucleation centers or CDW precursors above T_c (Weitering *et al.*, 1999). Scanning tunneling microscopy and spectroscopy (STM and STS) offer unparalleled capabilities of exploring the spatial variation of both amplitude and phase in reduced dimensionality. Specifically, one can visualize the important role of defects in establishing CDW order.

In this Colloquium we review recent observations and the current understanding of the structural and electronic instabilities in three different self-assembled wire arrays. Section III addresses the formation and properties of In atom wires on Si(111). In Sec. II, we discuss the electronic instabilities of Au-induced atom wires on stepped Si surfaces with different miscut angles. While similar and other atom wire systems have been discovered recently (see Sec. IV), the three systems highlighted are the ones that have been most thoroughly investigated.

II. GOLD-INDUCED QUASI-ONE-DIMENSIONAL ATOM WIRES ON SILICON SURFACES

A. Au/Si(111)

Many metallic elements form reconstructions on the Si(111) surface that are—at least structurally—quasi-1D. Many of these reconstructions consist of a parallel array of Si honeycomb chains that are separated by single wires of metal atoms (Erwin and Weitering, 1998). These honeycomb chains form a narrow strip of graphenelike (sp^2 bonded) Si [see Fig. 3(a)], and their frequent occurrence suggests that it is this building block that favors

symmetry breaking of the Si(111) substrate into quasi-1D domains. Moreover, the appearance of honeycomb chains in different metal-induced reconstructions with varying degrees of lattice strain suggests that this building block is quite stable.

Although the structure of the Si(111)- 5×2 -Au wire reconstruction is still not settled [cf. Yoon *et al.* (2005), Ren *et al.* (2007), and Chuang *et al.* (2008)], the most promising models (Erwin, 2003; Riikonen and Sánchez-Portal, 2005a; Ren *et al.*, 2007) suggest that this reconstruction also contains honeycomb chains. However, in contrast to the original honeycomb chain channel model featuring single rows of metal atoms (Erwin and Weiering, 1998), the Si(111)- 5×2 -Au reconstruction features two rows of Au atoms. STM images [see Fig. 3(b)] show two atom wires in a zigzag arrangement decorated with occasional Si adatoms (Erwin, 2003; Kirakosian *et al.*, 2003; McChesney *et al.*, 2004).¹ STS measurements revealed that wire segments featuring a local 5×4 adatom arrangement are semiconducting whereas segments without Si adatoms are metallic (Yoon *et al.*, 2004). The DOS of this atom wire array does not show a clear Fermi cutoff at room temperature but this is probably unrelated to Luttinger liquid physics and is more likely the consequence of disorder induced by the Si adatoms. Moreover, no phase transition has been observed in this system. Attention has therefore shifted to other Au-induced quasi-1D reconstructions on vicinal Si(111) surfaces (Stevens *et al.*, 1993; O'Mahony *et al.*, 1994; Jałochowski *et al.*, 1997), which do exhibit clear signs of electronic instabilities as discussed in the following sections.

B. Au/Si(557)

1. Atomic and electronic structure

Si(557) is a vicinal surface with its basal orientation tilted 9.5° away from the (111) surface toward the $[\bar{1}\bar{1}2]$ direction. Deposition of 0.18 monolayer (ML) of Au [1 ML = 7.8×10^{14} atoms/cm², the density of Si atoms in the bulk (111) plane] onto this surface at 650°C followed by a short postanneal at 850°C produces a regular array of single (111)-like steps and nanoscale (111) terraces (see Fig. 4). The terraces are 1.92 nm wide. The large wire spacing minimizes the interchain coupling so that this surface is almost perfectly 1D. Surface x-ray diffraction (XRD) experiments (Robinson *et al.*, 2002) indicated that (i) the structure contains only one Au atom per surface 1×1 unit cell, consistent with the estimated coverage from other experiments (Segovia *et al.*, 1999; Altmann *et al.*, 2001); (ii) this Au atom is substitutionally incorporated in the middle of the terrace; (iii) the Si-Au bond lengths are almost indistinguishable from the Si-Si bond lengths, consistent with a low strain substitutional location for the Au atoms; (iv) Si adatoms, one in every

¹Depending on experimental conditions, other structures have also been observed [see, e.g., O'Mahony *et al.* (1994)].

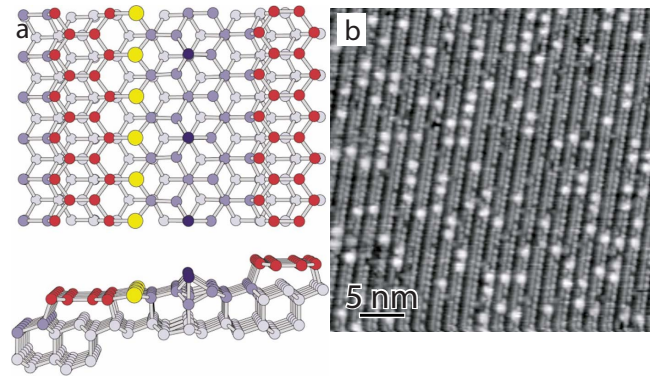


FIG. 4. (Color online) The Si(557)-Au reconstruction. (a) Structural model for Si(557)-Au. Large light circles are Au atoms, darker circles at the step edges are Si honeycomb atoms, very dark circles are Si adatoms. (b) STM image of the Si(557)-Au surface at room temperature. Tunneling voltage $V=1.5$ V; tunneling current $I_t=300$ pA. From Crain *et al.*, 2004 and Snijders, 2006.

other unit cell, each saturating three dangling bonds on the terrace; and (v) the step-edge atoms rebond producing Si-Si bond angles close to 120° , indicating the existence of honeycomb chains at the step edges. The precise step geometry is least understood. Thus the Si(557)-Au and the Si(111)- 5×2 -Au structures have similar building blocks, namely, a honeycomb chain, substitutional Au atoms embedded in the terraces, and Si adatoms. The structural model is shown in Fig. 4(a).

Segovia *et al.* (1999) reported angle-resolved photoemission spectroscopy (ARPES) measurements of the band structure. They observed a half-filled band dispersing along the wire direction crossing E_F [see Fig. 5(a)]. This state did not disperse in the direction perpendicular to the wires, confirming its 1D character. The single metallic state was believed to originate from the Au $6s$

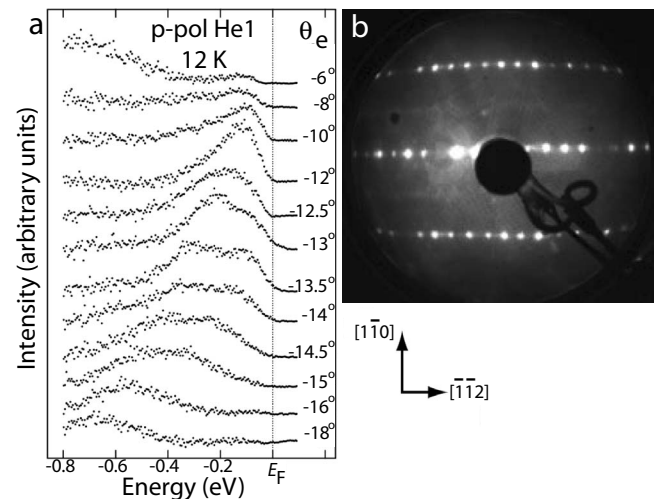


FIG. 5. Band dispersion and reciprocal lattice of Si(557)-Au. (a) ARPES spectra of Si(557)-Au, showing a split half-filled band dispersing to E_F . (b) LEED pattern of the surface, revealing an ordered anisotropic structure. From Segovia *et al.*, 1999.

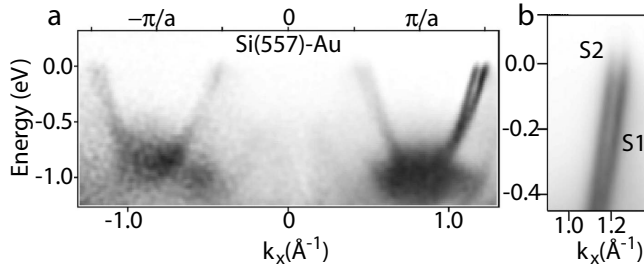


FIG. 6. Band structure of the Si(557)-Au surface measured with ARPES. (a) Full Brillouin zone along k_x , with the zone boundaries at π/a and (b) a zoom-in image of the doublet of S1 and S2 bands. Adapted from Altmann *et al.*, 2001 and Crain *et al.*, 2003.

level. Three key observations were made in this paper. First, using low-energy electron diffraction (LEED) no changes in the symmetry and periodicity of the atom wire structure were observed between 60 and 300 K [see Fig. 5(b)]. The symmetry of the bands also did not change between 12 and 300 K. Second, no clear Fermi cutoff was observed. Instead, the photoemission intensity below E_F followed a power-law behavior. Finally, the dispersing band was split into two bands over a wide energy range and these two states seemed to merge into a single peak near E_F . These observations seemed to suggest that the atom wire array exhibits the distinctive characteristics of the spinon and holon collective excitations in a Luttinger liquid (Segovia *et al.*, 1999).

Later photoemission studies of the Si(557)-Au with better resolution (Losio *et al.*, 2001; Ahn *et al.*, 2003) showed that the two dispersing states did not merge at E_F (see Fig. 6). Instead two close but separate Fermi crossings were observed located halfway out to the $n \times 1$ Brillouin-zone boundary. The crossings are symmetric about the $n \times 2$ zone boundary (Losio *et al.*, 2001). The separate crossings invalidate the proposed Luttinger liquid interpretation for this system (Losio *et al.*, 2001). Note, however, that the dispersion of a 1D plasmon in these atom wires as measured with electron energy loss spectroscopy (EELS) (Nagao *et al.*, 2006) indicated significant exchange correlations. Electron correlations therefore do play a measurable role in this system.

The presence of two half-filled bands S1 and S2 (Fig. 6) also seemed to solve the puzzling fact that the surface is metallic in spite of the even electron count resulting from the seven half-filled dangling bonds (five at the terrace and two at the step edge) and one Au 6s electron per bulk terminated Si(557) 1×1 unit cell. Note, however, that the reported band fillings of S1 and S2 differ slightly (Losio *et al.*, 2001; Ahn *et al.*, 2003; Crain *et al.*, 2004). These differences were attributed to slightly different coverages of the Si adatoms, which presumably act as dopants (Crain *et al.*, 2004). Here we use the data from Crain *et al.* (2004) with band fillings of 0.42 and 0.49 for S2 and S1, respectively. Generally, the reported band fillings do not add up to integer electron counts per unit cell, consistent with a defect-doping picture. How-

ever, noninteger total band fillings could also indicate that the actual unit cell of the system is larger than experimentally observed.

Finally, we note that weak oscillations in the quasi-1D Fermi contours measured by ARPES indicate weak two-dimensional (2D) coupling. The ratio of the parallel and transverse hopping integrals t_{\parallel}/t_{\perp} was determined from a tight-binding fit to the Fermi contour and is ≥ 60 (Crain *et al.*, 2004). The well-known quasi-1D Bechgaard salts only have a ratio of ~ 10 , and the Si(557)-Au surface thus indeed represents a good approximation to an ideal 1D metallic system.

STM images such as Fig. 4(b) reveal two atomic wires per unit cell parallel to the step edges with occasional bright protrusions on top of the wires (Losio *et al.*, 2001; Ahn *et al.*, 2003; Yeom *et al.*, 2005; Krawiec *et al.*, 2006). One atomic wire has a highly corrugated $\times 2$ periodicity, which dominates in empty state STM images (Losio *et al.*, 2001). Moreover, this atom wire appears to be insulating in room temperature STS experiments (Yeom *et al.*, 2005). The second wire is dominant in the filled state images. It has little noticeable corrugation at room temperature. STS measurements indicate that this wire is metallic at room temperature (Yeom *et al.*, 2005). Comparison of the interchain spacings in STM images with the structural model from XRD studies suggests that the insulating “atomic” wire is comprised of Si adatoms and that the metallic wire is formed by dangling bonds of the step-edge Si atoms (Robinson *et al.*, 2002).

STM images reveal occasional bright protrusions on top of the double wire unit cell and voids mainly in the adatom wire. Analogous to the Si(111)- 5×2 -Au surface, these bright protrusions could be additional Si adatoms. In this respect, two scenarios could exist for the proposed defect-doping mechanism mentioned above: hole doping reducing the band filling to below 50% or electron doping in which defects fill the initially empty or quarter-filled (amounting to a total filling of one electron) bands to the ~ 0.45 filling. Note that the concentration of defects in STM images is fairly large—on the order of 10% (Losio *et al.*, 2001; Crain *et al.*, 2004)—which could correlate with the $\sim 10\%$ deviation of the ~ 0.45 filling of a half-filled parent band structure.

In conclusion, even though Si(111)- 5×2 -Au and Si(557)-Au appear to have similar building blocks, there are important differences in their electronic structures. As discussed in the following sections, this is likely related to the most important structural difference between the two, namely, the presence of a step edge in each Au/Si(557) unit cell and the associated larger structural degrees of freedom. Only Au/Si(557) exhibits an electronic instability and insulator-metal transition.

2. Metal-insulator transition

In contrast to the report of Segovia *et al.* (1999), a detailed *temperature-dependent* ARPES and STM study by Ahn *et al.* (2003) showed that a symmetry-breaking metal-insulator transition does in fact occur with a T_c of ~ 270 K, precluding the formation of a Luttinger liquid

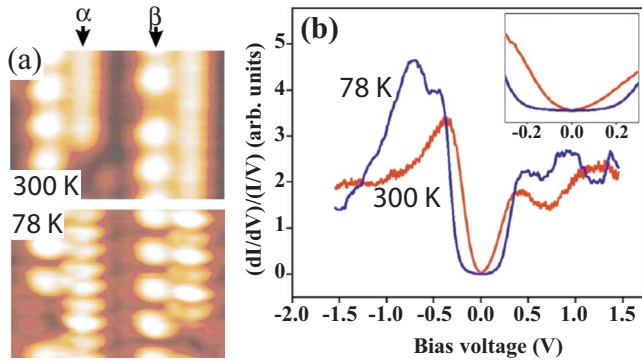


FIG. 7. (Color online) STM and STS data from the Si(557)-Au surface. (a) STM images ($V=1$ V) and (b) STS normalized dI/dV data of Si(557)-Au at 300 and at 78 K revealing a doubling of the periodicity in the step-edge wire and the appearance of a gap at low temperature. The inset in (b) is a zoomed-in spectrum near zero bias. From Ahn *et al.*, 2003 and Yeom *et al.*, 2005.

at low temperature. Figure 7(a) shows STM images taken at room temperature and at 78 K. A clear doubling of the periodicity corresponds to an “up-down” corrugation in the metallic step edges at low temperature. Low-temperature ARPES measurements show a gap in $S1$ close to the $n \times 2$ Brillouin-zone boundary. In addition, ARPES data show that the leading edge of this band shifts by up to 40 meV with decreasing temperature. Assuming that the gap is symmetric around E_F , this would indicate a gap of $2\Delta=80$ meV at 78 K, consistent with local STS measurements on the step-edge wire (Yeom *et al.*, 2005). The temperature dependence of the measured gap is reasonably well fitted by the mean-field gap equation [cf. Grüner (1994)], resulting in a mean-field T_c of 260 K (Ahn *et al.*, 2003). These data were interpreted in terms of a traditional Peierls transition in the $S1$ band due to its near-perfect nesting. The zero-temperature CDW coherence length can be estimated from this gap and Fermi velocity (Crain *et al.*, 2003) using BCS theory (Grüner, 1994), resulting in $\xi \approx 5$ nm. This amounts to approximately seven doubled unit cells along the wire. In the classical Peierls picture, this correlation length lies in between that of a strongly coupled system where the correlation length is no longer than a few unit cells and that of a weakly coupled system where the correlation length can be hundreds of unit cells long. The quite good agreement between the magnitude of the experimental gap and T_c is surprising because the $S1$ band is highly 1D (meaning that mean-field theory should fail due to strong fluctuations) and because the electron-phonon coupling appears to be quite strong. Note, however, that the assumption of a symmetric gap may not be correct.

Contrasting with the observed gap opening in $S1$, Ahn *et al.* (2003) observed that the $S2$ band is already gapped at room temperature, with a partial gap below E_F of about 50 meV, which is possibly caused by a similar phase transition above room temperature. A symmetric gap of 100 meV would correspond to a T_c of 329 K

within the mean field framework, consistent with the hypothesis that the transition occurs above room temperature. However, the room temperature gap in $S2$ has not been independently confirmed with ARPES [cf. Losio *et al.* (2001), Crain *et al.* (2004), and Barke *et al.* (2006)] although similar claims were made by the same group for the Si(553)-Au surface (see Sec. II.C.1) and Si(337)-Au (Ahn, Yeom, *et al.*, 2004). EELS experiments by Nagao *et al.* (2006) supported the existence of a gap in one of the two half-filled bands at room temperature. In this respect, it is interesting to note that only the data of Ahn *et al.* (2003) showed an $S2$ band that would be exactly half filled if the measured dispersion is extrapolated to E_F (see also Sec. II.C.3).

Another issue that could play a role here was suggested by Starowicz *et al.* (2002). They demonstrated that defects can produce a photoelectron spectrum that is very similar to that of a Luttinger liquid. In atom wires with defects, photoelectrons originate from isolated wire segments that are metallic. The photoelectrons experience a charging shift, whose magnitude depends on the length of the segment. The resulting kinetic-energy distribution resembles the power-law distribution for interacting 1D systems. The gap determination would thus become inaccurate. It is unclear, however, why only one of the two bands would be affected.

The interpretation of this metal-insulator transition in terms of a single-band Peierls mechanism has been under debate (Ahn *et al.*, 2003; Sánchez-Portal *et al.*, 2004; Yeom *et al.*, 2005; Riikonen and Sánchez-Portal, 2007). The main topic of the debate hinges on the origin of the nearly half-filled doublet of bands. If the metal-insulator transition is similar to a classical Peierls distortion, then the $S1$ band should be located at the step edge, doubling its periodicity at low temperature so as to be consistent with the STS data of Yeom *et al.* (2005). On the other hand, $S1$ should be located in the middle of the terrace if it originates from Si-Au bonds as proposed by Sánchez-Portal *et al.* (2004) and Riikonen and Sánchez-Portal (2007) and discussed in the next section.

3. Alternative model of the transition

Using first-principles density functional theory (DFT) calculations and molecular dynamics simulations, Sánchez-Portal *et al.* (2004) and Riikonen and Sánchez-Portal (2007) provided an alternative, microscopic view of the phase transition. The proposed mechanism also features a strong interaction between the electronic and atomic degrees of freedom, but in contrast to the conventional Peierls mechanism this interaction is “nonlocal” in nature: the amplitude of a structural distortion at the step edge controls the position of the Fermi level, which in turn drives a metal-insulator transition in bands that are localized in the middle of the terrace.

The electronic structure of the Si(557)-Au surface was calculated within a relaxed structural model that is similar to the model derived from XRD (Robinson *et al.*, 2002). The results indicate that the electronic band associated with the step-edge atoms has a very small disper-

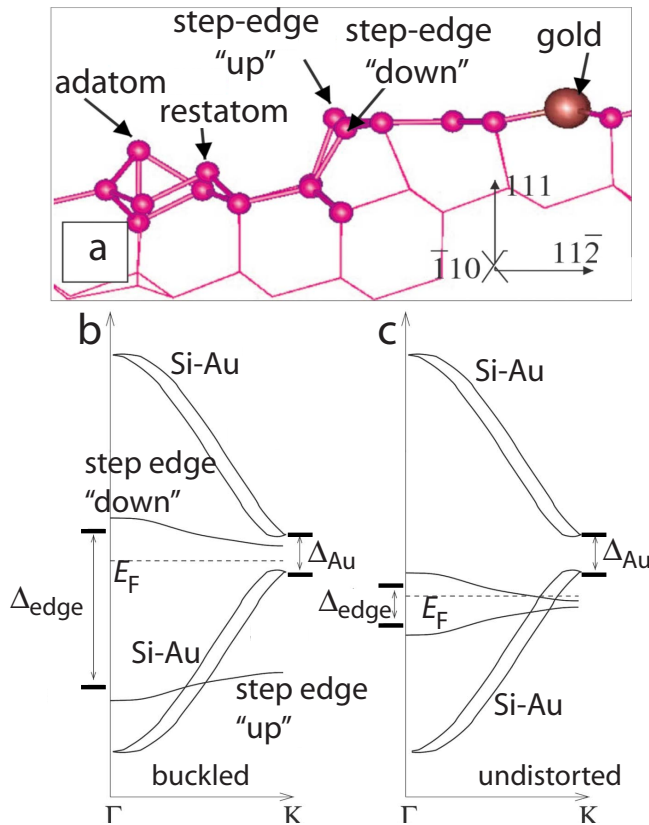


FIG. 8. (Color online) Model of the order-disorder transition in Si(557)-Au surface. (a) Detailed structural model of the Si(557)-Au surface showing buckled step-edge atoms. Schematic band structure (b) below and (c) above T_c , showing the empty step-edge bands and energy gap in the spin-split Si-Au bands. Adapted from Riikonen and Sánchez-Portal, 2007.

sion and thus cannot be identified with the split parabolic bands in ARPES (Ahn *et al.*, 2003). Calculations indicate that the band splitting should be attributed to spin-orbit coupling in bands that are associated with the Si-Au bonds. A crude estimate from published data (Ahn *et al.*, 2003; Crain *et al.*, 2003) indicates a spin-orbit splitting of >200 meV at E_F , i.e., twice as large as the splitting of the 2D surface state on Au(111) (LaShell *et al.*, 1996). The total filling of this spin-split doublet thus amounts to 0.45(5) [the average of the reported two separate fillings of 0.42 and 0.49 (see Sec. II.B.1)].

In the model by Sánchez-Portal *et al.* (2004) and Riikonen and Sánchez-Portal (2007), summarized in Fig. 8, the Si-Au-derived bands exhibit a small band gap at the zone boundary. This gap opening is caused by the $\times 2$ ordering of Si adatoms on the same terrace, which induces an alternation of the Si-Au bond angle along the Si-Au wire. The Si atoms at the step edge undergo a vertical buckling distortion, creating a gap between the filled (up) and empty (down) dangling-bond-derived bands. With decreasing temperature the buckling amplitude grows, increasing the gap between the filled and empty step-edge bands and rendering the system insulating [see Fig. 8(b)]. This would explain the nonmetallic properties of the step-edge atoms and the $\times 2$ periodicity

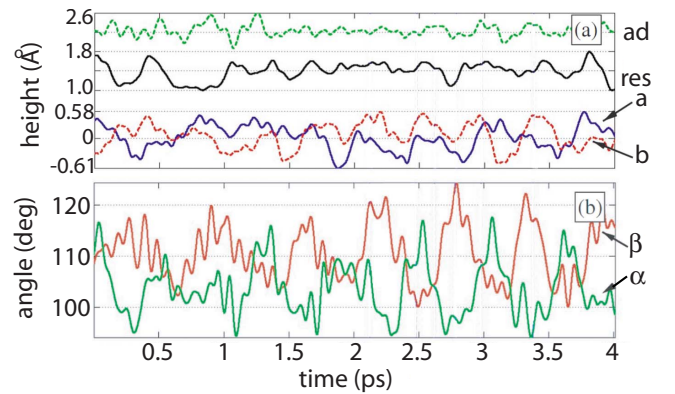


FIG. 9. (Color online) Final 4 ps (of a total of 8 ps) of a molecular dynamics simulation of the Si(557)-Au reconstruction performed at ~ 300 K. (a) The height of different atoms as a function of time (see also Fig. 8): adatom (*ad*, dashed line), rest atom (*res*, solid line), and the step-edge atoms (*a*, solid line and *b*, dashed line). (b) The two inequivalent Si-Au-Si bond angles (α and β). Adapted from Riikonen and Sánchez-Portal, 2007.

seen in low-temperature STM (Ahn *et al.*, 2003; Yeom, *et al.*, 2005). Note that in the semiconducting state at low temperature, the Si-Au split bands are completely filled and thus contain a total of two electrons. Combined with the two electrons in the “up” band at the step edges, the model satisfactorily explains the even electron count of a $\times 1$ unit cell at the Si(557)-Au surface (cf. Sec. II.B.1).

Using first principles molecular dynamics simulations Sánchez-Portal *et al.* (2004) and Riikonen and Sánchez-Portal (2007) showed that the buckling of the step-edge atoms and the Si-Au bond angles fluctuate significantly at high temperatures so that the system spends a considerable amount of time in intermediate structural configurations (see Fig. 9). Consequently, the average gap in the step-edge bands decreases and the time-averaged position of the “down” band shifts to lower energy. The Si-Au gap also decreases for this configuration because the Si-Au bond angles that are inequivalent at low temperature become on average more equivalent at high temperature. However, the gap at the $\times 2$ zone boundary in the step-edge band does not close completely and the step-edge wire seems to undergo an “order-disorder” transition. The metal-insulator transition occurs when the empty step-edge band crosses the Si-Au bands. The down band then becomes partially filled due to the charge spilling from the Si-Au bands [see Fig. 8(c)]. Because of its small dispersion, the down band effectively pins the Fermi level. This model adequately explains the noninteger band filling of the doublet observed in ARPES experiments at room temperature.

Simulated STM images at both high and low temperatures show reasonable agreement with experimental data (Riikonen and Sánchez-Portal, 2007). Also, the calculated step-edge DOS shows fair agreement with the experiments although the calculations produce a partial filling of the down step-edge band even below T_c . This was attributed to an artifact of the DFT calculation and is not observed in experimental STS data (Yeom *et al.*,

2005; Riikonen and Sánchez-Portal, 2007). Note that the metallic Si-Au bands do not seem to contribute to the STM images and their role in the STS data is not clear. The absence of these metallic bands in the STM data may be due to the fact that the Si-Au bands cross E_F at the large parallel wave vector while STM experiments are more sensitive to states at the center of the Brillouin zone.

There are several conflicting issues with this scenario (Yeom *et al.*, 2005; Riikonen and Sánchez-Portal, 2007). Experimental STS curves at low temperature indicate that a *symmetric* gap has opened up at the step edges. Furthermore, the STS data do not reveal metallicity at locations other than the step edges (Yeom *et al.*, 2005). This contradicts the theory result, which indicated a strongly asymmetric band gap opening at the step edges as well as the existence of a metallic Si-Au band in the middle of the terrace [Fig. 8(b)]. Another problem is that the flat step-edge bands have not been seen in photoemission experiments, although this could possibly be explained by assuming a low photoemission cross section for this band (Crain and Himpfel, 2006). In addition, the hopping ratios t_{\parallel}/t_{\perp} of the two parabolic bands differ by more than 20% (Crain *et al.*, 2003), which seems hard to reconcile with the ideal picture of a nearly free-electron system perturbed by the Rashba interaction (Sánchez-Portal *et al.*, 2004; Riikonen and Sánchez-Portal, 2007), indicating that the band structure could be more complicated. In principle, this leaves room for alternative interpretations of the band splittings. Finally, the observation of a room temperature gap in only one of the split bands by Ahn *et al.* (2003), and indirectly in the EELS study of Nagao *et al.* (2006), is not reproduced in the scenario of Sánchez-Portal *et al.* (2004) and Riikonen and Sánchez-Portal (2007). On the other hand, the EELS study of Si(557)-Au (Nagao *et al.*, 2006) and photoemission experiments of Si(553)-Au (featuring a similar doublet of bands) do seem to corroborate the spin-orbit coupling picture (Barke *et al.*, 2006) (see also Sec. II.C.1). Note that Coulomb interactions in the atom wires could also lead to charge ordering at low temperature. However, none of the proposed models explicitly addresses the role of these interactions in the transition. In spite of these issues and barring an unlikely significant spin-orbit coupling at the Si step edge, the combined structural and electronic model proposed by Sánchez-Portal *et al.* (2004) and Riikonen and Sánchez-Portal (2007) is so far the only theoretical model showing fair agreement with STM and STS data and it is fully consistent with structure studies (Robinson *et al.*, 2002). The precise atomistic mechanism of the phase transition at $T_c=260$ K is still under debate and more detailed experiments are necessary to reconcile experimental observations pointing toward the classical Peierls picture, as advocated by Ahn *et al.* (2003) and Yeom *et al.* (2005), and those that seem to confirm the more complex scenario by Riikonen and Sánchez-Portal (2007).

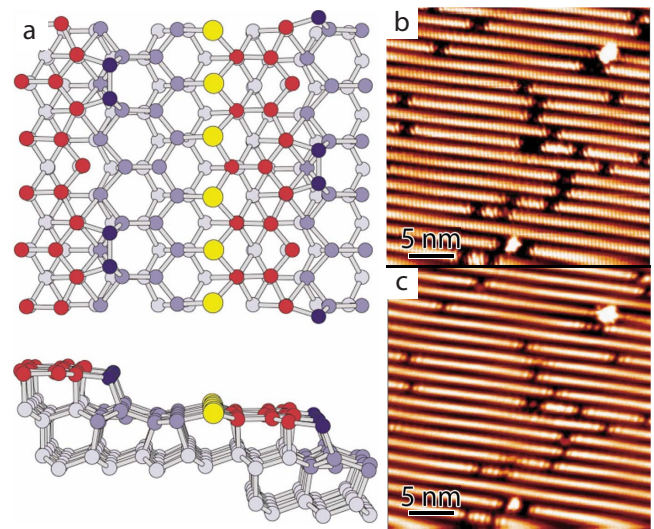


FIG. 10. (Color online) The Si(553)-Au reconstruction. (a) Structural model for the Si(553)-Au. Atoms indicated as in Fig. 4. (b) Empty state and (c) filled state STM images of the Si(553)-Au surface at room temperature. $V \pm 0.5$ V, $I_t = 50$ pA. From Crain *et al.*, 2004 and Snijders *et al.*, 2006.

C. Au/Si(553)

1. Atomic and electronic structure

In search for atom wire arrays with different inter-chain couplings, other vicinal Si surfaces have been investigated. In a comprehensive experimental search, it was found that only surfaces with odd Miller indices form well-ordered step arrays after depositing Au (Crain *et al.*, 2004). The Si(553) surface is one of these. It has a vicinal angle that is tilted toward the $[11\bar{2}]$ direction. The tilt angle is larger than that of the Si(557) surface and, consequently, the terrace width is smaller (1.48 nm). A larger amount of 0.24 ML Au is required in order to produce an ordered array of atom wires as observed with STM [see Figs. 10(b) and 10(c)].

ARPES measurements reveal an intriguing band structure (see Fig. 11) (Crain *et al.*, 2003). It consists of a doublet of bands ($S1$ and $S2$) very similar to the two bands observed for the Si(557)-Au surface. The bands cross E_F at wave vectors corresponding to 0.51 and 0.56

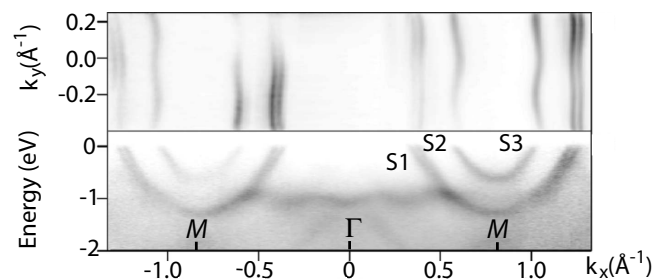


FIG. 11. Electronic structure of the Si(553)-Au reconstruction. Band dispersion (bottom) and Fermi surface (top) of the Si(553)-Au surface as measured by ARPES. Adapted from Crain *et al.*, 2003.

fractional fillings of the bands. In addition a third band, S_3 , with a fractional filling of 0.27 is observed. The total filling thus adds up to $\frac{4}{3}$, which equals $\frac{8}{3}$ electrons per unit cell, the key assumption being that the three bands are spin degenerate. Their minima are all located at the M point in the Brillouin zone. Similar to the Si(557)-Au surface (Sec. II.B.1), the electron count of the structure model shown in Fig. 10(a) is even. Here four electrons originate from the four half-filled dangling bonds on the terrace, one from the dangling bond at the step edge, and one from the Au 6s level. This even electron count is at odds with the experimentally observed fractional band fillings. Crain *et al.* (2003) suggested that this fractionally filled band structure could become very interesting when electron correlations are strong: electron correlations in a half-filled band could open up a Mott-Hubbard gap, thus producing a 1D Mott insulator. For a quarter-filled band with vanishing nearest-neighbor Coulomb interaction, one would instead obtain a highly correlated 1D metal where the Fermi level resides inside the lower Hubbard band. [A gap opening might be realized by switching on interatomic Coulomb interactions, as in the case of some Bechgaard salts with quarter-filled bands (Voit, 1995).]

The Fermi contours exhibit some wiggling. A detailed tight-binding model analysis of the Fermi contour (see Fig. 11) (Crain *et al.*, 2003, 2004) showed that the hopping ratios $t_{||}/t_{\perp}$ are ~ 46 , ~ 39 , and 12 for S_2 , S_1 , and S_3 , respectively. Compared to the Si(557)-Au surface where the hopping ratios for S_1 and S_2 are >60 , the interwire coupling on Si(553)-Au is clearly stronger, with S_3 approaching that of the Bechgaard salts (cf. Sec. II.B.1). This is consistent with the smaller unit cell width on Si(553)-Au. Indeed, for four different Au-induced atomic wire arrays on vicinal Si exhibiting a similar doublet of bands, the interwire coupling correlates inversely with the atom wire spacing (Crain *et al.*, 2004). It thus appears possible to tune the 2D interwire coupling by changing the vicinal angle of the Si substrate. The band filling itself is also a function of the vicinal angle, though this relation is not monotonic, possibly due to the appearance of the third band in some of these systems.

As mentioned in Sec. II.B.3, Barke *et al.* (2006) showed experimentally that S_1 and S_2 are in fact (Rashba) spin-orbit split bands. Detailed ARPES measurements reveal that both bands are backfolded near the 2×1 zone boundary (see Fig. 12). Because the bands cross E_F slightly beyond the zone boundary, the backfolded bands cross the original bands. The interaction between bands with the same quantum numbers produces avoided crossings in their dispersion. From the pattern of avoided crossings, Barke *et al.* (2006) demonstrated that the doublet of bands arises from spin-orbit splitting, confirming earlier theoretical work (Sánchez-Portal *et al.*, 2004; Riikonen and Sánchez-Portal, 2007). Consequently, the total filling of this doublet of bands is $(0.51+0.56)/2=0.53(5)$, slightly larger than that of the spin-split doublet on Si(557)-Au (Crain *et al.*, 2003), amounting to a total band filling of $0.53+0.27=0.80$ (S_3

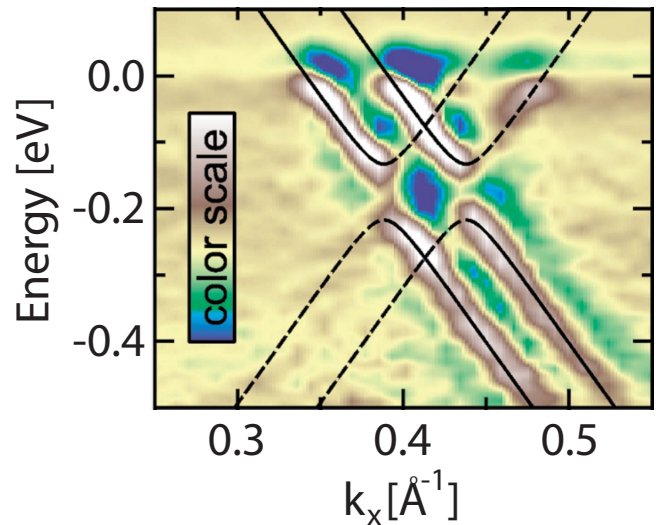


FIG. 12. (Color online) High-pass filtered high-resolution band dispersion of the doublet of bands close to the $\times 2$ zone boundary at 0.41 \AA^{-1} revealing a pattern of horizontally displaced avoided crossings. Adapted from Barke *et al.*, 2006.

remains spin degenerate). This band filling does not correspond to an integer number of electrons per surface unit cell, which suggests either a surface doping mechanism or a quintupling of the unit cell. However, there is no experimental indication of such a large unit cell. Note that also similar to the case of Si(557)-Au, a puzzling but significant difference of $>10\%$ exists in the interwire coupling of the two spin-split bands for Si(553)-Au. Moreover, Ahn *et al.* (2005) reported that the inner band of the doublet displays a (partial) gap of ~ 40 meV, similar to their findings for Si(557)-Au (Sec. II.B.1). These observations, which have not been independently confirmed, are hard to reconcile with the proposed Rashba splitting (Sánchez-Portal *et al.*, 2004; Barke *et al.*, 2006).

Several studies were aimed at elucidating the structure of the Si(553)-Au atom wire array, but so far STM studies have provided the most detailed information for direct comparison with theoretical *ab initio* calculations.² Room temperature STM images show bright lines separated by dark “channels” (see Fig. 10) (Crain *et al.*, 2004, 2006; Ahn *et al.*, 2005; Crain and Pierce, 2005; Snijders *et al.*, 2006; Ryang *et al.*, 2007). Defects that appear as vacancies cut the bright lines into segments. The empty state images generally reveal some more detail, but overall there are no large variations with STM bias polarity. Both the bright wires and the dark channels exhibit a $\times 1$ periodicity of 3.84 \AA at room temperature, although a local $\times 2$ periodicity is occasionally observed in the channels at room temperature (Crain *et al.*, 2003;

²There is a report on x-ray diffraction of Si(553)-Au (Ghose *et al.*, 2005). However, the relevance of this study for the present discussion is uncertain because the Au coverage of Ghose *et al.* (2005) is twice as large. Moreover, the proposed structure was later found to be thermodynamically unstable (Riikonen and Sánchez-Portal, 2006; Ryang *et al.*, 2007).

Ahn *et al.*, 2005; Crain and Pierce, 2005).³

Based on the STM observation of a $\times 3$ ordering of vacancylike defects in wires with high defect density, Crain *et al.* (2003, 2004) suggested (before the role of Rashba splitting was recognized) that a fluctuating pair of Si adatoms per three unit cells could explain the $\frac{8}{3}$ electron count. Later theoretical studies (Riikonen and Sánchez-Portal, 2005b, 2008; Ryang *et al.*, 2007) concluded that, in contrast to the Si(557)-Au surface, there are no Si adatoms on the Si(553)-Au surface because there is insufficient room on the smaller terraces to accommodate them (Ghose *et al.*, 2005). The absence of adatoms is consistent with STM images which do not show the characteristic adatom protrusions. Note that the absence of Si adatoms leaves a row of unsaturated dangling bonds on the terrace (Riikonen and Sánchez-Portal, 2008). This is a major difference with the Si(557)-Au surface, which could explain the appearance of S_3 on Si(553)-Au.

Most first-principles calculations and, in particular, the extensive systematic study of over 200 structural models in Riikonen and Sánchez-Portal (2008) indicate that the step edge in each unit cell is terminated with a Si honeycomb chain and that the single wire of Au atoms is substitutionally incorporated in the terrace, similar to the case of Si(557)-Au (Crain *et al.*, 2004; Riikonen and Sánchez-Portal, 2005b; Ryang *et al.*, 2007) (see Figs. 4 and 10). The similarity of the half-filled spin-orbit split bands S_1 and S_2 in Si(557)-Au and Si(553)-Au strongly supports this view. On the other hand, bulk-truncated step edges on surfaces such as Si(553) that are vicinal toward $[11\bar{2}]$ have only one broken bond at the step edge, whereas surfaces that are vicinal toward $[\bar{1}\bar{1}2]$ such as Si(557) have two broken bonds (Crain *et al.*, 2004). It is thus somewhat unexpected that for both vicinal surfaces, having fundamentally different unreconstructed step-edge structures, honeycomb chains seem to provide the lowest energy structure for both types of step edges. STM image simulations based on these proposed structural models consistently indicate that the bright wire corresponds to the honeycomb chain and that the observed $\times 1$ periodicity in the dark channel likely originates from the Au atoms on the terrace (Ryang *et al.*,

2007; Riikonen and Sánchez-Portal, 2008).⁴ Therefore, in contrast to the Si(557)-Au surface where only the adatom and step-edge Si atoms are imaged, Au atoms can be imaged in the Si(553)-Au structure, provided of course that the structure model of Riikonen and Sánchez-Portal (2007) is correct.

Band-structure calculations of the most promising models by Riikonen and Sánchez-Portal (2008) show, in addition to a spin-split doublet of bands, an $\sim \frac{1}{5}$ -filled band that originates from the row of dangling bonds on the terrace. This band resembles the experimentally observed S_3 band. However, in these calculations all bands exhibit significant spin splitting. This is inconsistent with the ARPES experiments, which only show a spin splitting in the half-filled band. In the models studied by Riikonen and Sánchez-Portal (2008), the specifics of the band structure are determined by the exact location of the Au atoms: due to the large electron affinity of both the Au atoms and the honeycomb chain, they control the filling of the dangling bonds on the terrace and at the step edge. Small structural changes near the Au atoms and honeycomb chain can result in the (dis)appearance of a metallic band (Riikonen and Sánchez-Portal, 2008). However, none of these models convincingly mimics the experimentally observed band filling.

A different set of reconstructions was also explored by Riikonen and Sánchez-Portal (2008) in which part of the terrace reconstructs into a π -bonded chain. These π -bonded chain models also tend to incorporate honeycomb chains, but they would be located in the middle of the terrace. To reach a low energy, the structure at the step edge is strongly modified. These models show fair agreement with photoemission data showing one spin-orbit split band and an additional metallic band with lower filling, but the features in STM image simulations are hard to identify with those observed in experimental images.

2. Metal-insulator transitions in multiple bands

When cooling the Si(553)-Au atom wire surface to low temperatures, STM and LEED images reveal multiple commensurate lattice distortions (Ahn *et al.*, 2005; Snijders *et al.*, 2006) (see Fig. 13). At the lowest temperatures accessed with STM (~ 40 K), the system features two coexisting periodic lattice distortions within a single unit cell: the bright (step-edge) wires show a $\times 3$ periodicity and the darker channels in between reveal a $\times 2$ periodicity. One report (Snijders *et al.*, 2006) also observed a third $\times 2$ periodicity at intermediate temperatures (~ 110 K) located on the bright wires. This distur-

³Note that one study reported a zigzag structure in the empty state images at room temperature and a “ladder” structure in filled state images of the bright wire, both with a periodicity of 3.84 \AA (Snijders *et al.*, 2006). This was later attributed to a double tip effect (Ryang *et al.*, 2007) because Snijders *et al.* (2006) had not observed these features below T_c . However, the different *symmetries* of the zigzag and ladder structures observed *simultaneously* and with the same tip in dual bias images rule out a double tip effect. Moreover, as discussed in Sec. II.C.2, low-temperature images show a considerably modified structure with a much higher corrugation, and it should thus not be surprising that the faint zigzag and ladder corrugations from the room temperature images are not visible below T_c .

⁴As a note of caution, notice that in simulated STM images the $\times 1$ periodicity in the dark channel is rather weak and that the simulations show multiple faint features inside the dark channels depending on the tunneling bias (Riikonen and Sánchez-Portal, 2007). Obtaining the correct relative corrugations of different structural units is notoriously difficult in the Tersoff-Hamann simulations that were employed [see also Snijders *et al.* (2005)].

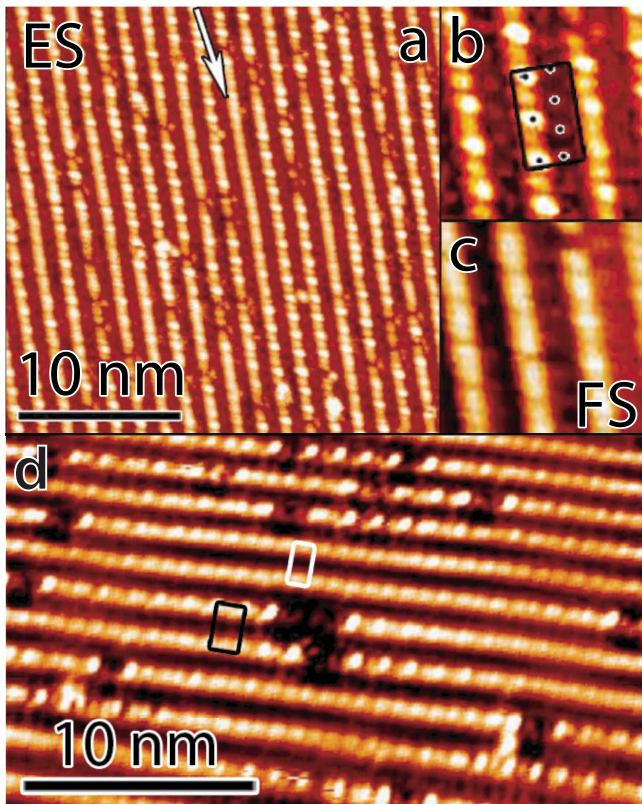


FIG. 13. (Color online) Variable temperature STM images of the Si(553)-Au reconstruction. (a) and (b) Empty state and (c) filled state STM images of the Si(553)-Au surface at 40 K, revealing $\times 3$ periodicities that are in antiphase in filled and empty state images. (d) Empty state STM image at 110 K showing both $\times 2$ (white) and $\times 3$ (black) unit cells. $V = \pm 1$ V, $I_t = 100$ pA for (a)–(c) and 1 V, 50 pA for (d). Adapted from Snijders *et al.*, 2006.

tion was seen to compete with the $\times 3$ periodicity that eventually covers the full length of the bright wires at the lowest temperatures [see Fig. 13(d)]. STS experiments [see Fig. 14(a)] reveal a metallic DOS at room temperature and an insulating DOS with a ~ 150 meV

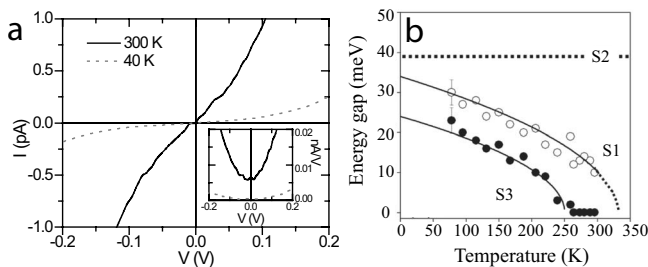


FIG. 14. Metal-insulator transition in the Si(553)-Au reconstruction. (a) STS I - V and dI/dV - V curves at room temperature and 40 K showing a metal-insulator transition on the Si(553)-Au surface. (b) Temperature dependence of the (partial) energy gaps of the three bands at the Si(553)-Au surface. $S1$ and $S2$ are the outer and inner bands of the doublet and $S3$ is the quarter-filled band. $S1$ and $S3$ are fitted with the BCS function for a relatively weak electron-phonon coupling. Adapted from Ahn *et al.*, 2005 and Snijders *et al.*, 2006.

gap (i.e., $dI/dV=0$ and $I=0$) at 40 K (Snijders *et al.*, 2006). The high-temperature band fillings of the quasi-1D bands are close to $\frac{1}{2}$ and $\frac{1}{3}$ fillings. Considering also the antiphase registry of the tripled periodicities in the filled and empty state STM images, it was concluded that these phase transitions are nesting induced, similar to the original proposal for the single CDW of Si(557)-Au (Ahn *et al.*, 2005; Snijders *et al.*, 2006).

The experiments discussed in this section were performed before the Rashba splitting of $S1$ and $S2$ was experimentally confirmed (Barke *et al.*, 2006), and as such their interpretations reflect the idea that the doublet consists of two spin-degenerate bands. We review them in the same context; in Sec. II.C.3 the consequences of the spin splitting on the interpretation of these data will be discussed.

ARPES measurements also indicate gap openings at low temperatures (Ahn *et al.*, 2005) [see Fig. 14(b)]. However, the gaps inferred from the ARPES data are much smaller. At room temperature, $S2$ has a gap that extends to 40 meV below E_F . This gap does not change upon cooling [Fig. 14(b)]. At 70 K, $S1$ and $S3$ have partial gaps extending 30 and 23 meV below E_F , respectively. However, the gradual opening of these gaps is still not completed at 70 K (Ahn *et al.*, 2005). Extrapolated BCS fits to the temperature-dependent gap data of $S1$ and $S3$ indicate 0 K (partial) gap values of 34 and 24 meV, respectively. The full gap values would be 68 and 48 meV if the gap openings were symmetric with respect to E_F . The BCS fits furthermore provide mean-field estimates of T_c 's, which are ~ 250 K for $S3$ and 350 K for $S1$, consistent with the observed backfolding at the 1×2 zone boundaries already at room temperature (Ahn *et al.*, 2005). The ARPES observations thus consistently point toward the existence of multiple weak-coupling CDW transitions. Note that there is a considerable discrepancy between T_c of 260 K determined from the BCS fits to $S3$ and STM observations at 110 K that do not show an extended $\times 3$ corrugation, suggesting that its T_c should be lower than 110 K. The prevailing $\times 1$ symmetry in STM images of the valleys at room temperature, instead of the expected $\times 2$ periodicity, could be due to fluctuations of the CDW below its mean-field transition temperature.

Similar to the Si(557)-Au system, Ahn *et al.* (2005) reported that $S2$ is already gapped at room temperature, raising questions about the origin of period doubling on the bright wires observed at intermediate temperatures with STM (Snijders *et al.*, 2006). This $\times 2$ periodicity competes with the low-temperature $\times 3$ CDW. In this case, a mechanism beyond that of the conventional CDW picture is likely, especially in light of the fact that the $S2$ gap is independent of temperature. One might speculate that the $\times 2$ periodicity is related to the presence of fluctuating Si dimers at the step edge. The $\times 2$ periodicity might finally be overcome at low temperature by a $\times 3$ Peierls-like transition in the same row.

While the above observations have been interpreted in terms of CDW instabilities, details turn out to be

more complicated. The Fermi wave vectors do not match the *commensurate* CDW periodicities very precisely. The initially reported fractional band fillings are 0.27, 0.51, and 0.56 for S_3 , S_2 , and S_1 , respectively (Crain *et al.*, 2003), assuming that all three bands are spin degenerate. [The fractional filling of S_1 and S_2 becomes 0.53(5) in the Rashba picture that was later established (see Sec. II.C.1).] Thus the nesting picture is not so clear-cut. Although it is known that the wavelength of a CDW can be locked to a nearby commensurate periodicity (Schrieffer, 1973) if the electron-lattice coupling is strong, the mean-field BCS fits suggest a rather weak coupling. In particular, the Fermi level crossing of the S_3 band is relatively far away from the commensurate $\times 3$ periodicity. It could energetically be more efficient for this band to distort into an even $\times 4$ periodicity corresponding to a $\frac{1}{4}$ filling also because local interactions between the neighboring $\times 2$ and $\times 3$ density wave corrugations would no longer be frustrated. The observed commensurate $\times 3$ periodicity could be explained by assuming a transfer of 0.12 electron from the half-filled band to the one-third-filled band, changing the fillings of both bands to commensurate values and thus stabilizing commensurate CDWs (Snijders *et al.*, 2006).⁵

STM images at different temperatures show that the $\times 2$ periodicity in between the bright wires and the $\times 3$ periodicity on the wires emanate from defects in the wires (Snijders *et al.*, 2006; Ryang *et al.*, 2007) [see Fig. 13(d)]. It was suggested that these defects could induce the interband charge transfer, leaving the total band filling constant. Data of Crain and Pierce (2005) indeed indicate that defects do not act as conventional dopants: STS measurements were performed on very short step-edge wire segments of only three to five atoms long, and the analysis of the spatially resolved DOS did not reveal significant changes in the *total* DOS of the wire segment (and the binding energy of the electron states in the middle of the chain) even though the nominal “dopant concentration” should be very different for defect-bound wire segments of different lengths.

It is very puzzling to note that the published ARPES data at 70 K do not show backfolding of the S_3 band at the 1×3 zone boundary, even though LEED clearly indicated 3×1 periodicity at that temperature (Ahn *et al.*, 2005). Instead, S_3 is folded around the 1×2 zone boundary near 100 K (Crain *et al.*, 2004). On the one hand, this might indicate that the $\times 3$ lattice potential probed by LEED does not act strongly on the orbitals comprising S_3 . Honeycomb chains of both Si and carbon (i.e., graphene) are notoriously resistant to structural transitions. Therefore, these observations could indicate that the $\times 3$ periodicity visible in the STM experiments is purely an electronic density wave with minimal coupling

to the lattice, thus featuring a negligible lattice distortion. On the other hand, the fact that the $\times 3$ periodicity has been seen in both LEED and STM suggests a definite relation between electronic and lattice periodicities. Either way, the absence of $\times 3$ periodicity in one or more bands remains not understood.

Zero temperature CDW coherence lengths can be deduced within the BCS framework (Grüner, 1994) from the Fermi velocity (Crain *et al.*, 2003) and gap size (Ahn *et al.*, 2005). For Si(553)-Au they amount to ~ 7 nm for S_1 and ~ 9 nm for S_3 , corresponding to 18 and 24 (1×1) unit cells, respectively. For the S_1 band in Si(557)-Au the CDW coherence length is 5 nm, corresponding to 14 unit cells.⁶ It is interesting to observe that the bands with the largest 2D coupling exhibit the largest coherence length in their CDW phase. This might indicate a significant 2D character of Si(553)-Au due to the larger transverse coupling, resulting in a lower T_c , smaller gap, and a longer coherence length. On the other hand, the CDW coherence length could also simply be limited by the defects in the quasi-1D atom wires. Indeed, the CDW coherence length is of the same order as the structural correlation length observed in the STM images that is mostly determined by the defect density, which will be discussed in Sec. II.C.4.

3. The doublet of half-filled bands

In the discussion in Secs. II.C.2 and II.B.2 we assumed, following the cited papers, that the doublets of S_1 and S_2 bands in both Si(557)-Au and Si(553)-Au constitute a simple pair of spin-degenerate bands. As discussed, the observed periodic distortions have been interpreted as conventional CDW transitions. However, the probable spin-orbit split origin of the doublet (cf. Sec. II.B.3 and Fig. 12) can have profound consequences for the CDW nesting picture. In this section we discuss some of these consequences for the interpretation of the experiments.

The spin-orbit coupling in the Au-derived metallic surface-state bands of Si(557)-Au and Si(553)-Au is unusually large. This spin-orbit splitting introduces different scattering vectors for the spin and charge excitations across the Fermi surface. This, in principle, changes the nature of Fermi surface instabilities and could give rise to spin-density wave instabilities or a spin-Peierls transition (Psaltakis, 1985). On the other hand, it has been shown that strong spin-orbit interactions can significantly enhance electron-phonon coupling in two dimensions (Cappelluti *et al.*, 2007). Such enhanced electron-phonon coupling could push a possible CDW transition into the strong-coupling regime, which in turn might explain the observation of commensurate periodicities in spite of the incommensurate Fermi wave vectors. Either way, the strong spin-orbit coupling in both Si(557)-Au

⁵The later discovered Rashba splitting of S_1 and S_2 (see Sec. II.C.1) changes the electron count but it does not necessarily invalidate the proposed mechanism. However, it would prevent reaching the exact commensurate band fillings as proposed by Snijders *et al.* (2006).

⁶Here we multiply the gap from ARPES by a factor of 2. Gap values from STS would result in a correlation length of ~ 2.7 nm.

and Si(553)-Au will likely have a significant effect on their ground-state properties (Marin and Suhl, 1989).

The model by Sánchez-Portal *et al.* (2004) and Riiikonen and Sánchez-Portal (2007) for Si(557)-Au includes the spin-orbit splitting of the surface-state doublet. However, its phase-transition mechanism only addresses changes in the band filling while there are no significant band structure effects (cf. Sec. II.B.3). Nonetheless, this Rashba splitting could change the perspective of the multiple transitions observed in Si(553)-Au. For example, using the band-filling data of Crain *et al.* (2004), the nesting vectors of the *same-spin* bands in Si(553)-Au correspond to a real-space periodicity of $\times 1.87$. Thus, CDWs associated with the *S1* and *S2* bands should be strongly *incommensurate* with the lattice. Only the nesting vectors spanning the inner Fermi contours of the spin-orbit doublet are within 2% of the exact $\times 2$ periodicity. However, these branches have *opposite* spin. Phonon-mediated coupling between electrons and holes in these opposite branches is an unlikely mechanism for CDW formation because it would require a spin flip.

A phase-transition mechanism similar to the one proposed for Si(557)-Au by Sánchez-Portal *et al.* (2004) and Riiikonen and Sánchez-Portal (2007) seems unlikely. STM experiments on Si(553)-Au do not show a clear $\times 2$ periodicity at RT that is necessary to open up the gap in the Si-Au bands near the 1×2 zone boundary. The latter could in turn lead to a metal-insulator transition, depending on the adjustment of the Fermi level with temperature. The Si(557)-Au mechanism could only explain the observed phase transitions of Si(553)-Au if the defect-induced $\times 2$ periodicity in between the atom wires would open up a gap in the Si-Au bands before a possible 1×1 to 1×3 disorder-order transition of the step-edge atoms sets in. However, several issues remain unresolved in this model; many of them are similar to the case of Si(557)-Au. The even electron count of the structure is inconsistent with the fractional band filling in the experiment. There is no experimental confirmation of the existence of a (presumably flat) band that would be related to the up step-edge atoms. Finally, the experimental observation of a gap in only one of the two spin-split bands remains puzzling. A gap opening in spin-orbit split bands could also arise from a $\times 2$ spin-density wave (SDW) or, alternatively, a spin-Peierls transition. In the SDW mechanism, spin-up electrons couple with the spin-down holes across the Fermi contour. However, the period doubling seen in low-temperature STM images cannot be attributed to the formation of a $\times 2$ SDW because conventional STM only senses the charge-density corrugation (Grüner, 1994). A spin-Peierls distortion might occur if the coupling between the spin and lattice is sufficiently strong. This would produce a doubling of the structural periodicity that would be observable in STM. Both scenarios would produce a gap at the new Brillouin-zone boundary.

Ahn *et al.* (2003, 2005) reported a gap opening in the inner branches of the surface-state doublets of Si(557)-Au and Si(553)-Au [see Fig. 14(b)]. These re-

ports have not been corroborated by other groups (Losio *et al.*, 2001; Crain *et al.*, 2003, 2004), but a possible cause for the gap opening might be related to the fact that the data of Ahn *et al.* (2003, 2005) consistently locate the k_F 's of the inner branches at almost exactly the 1×2 zone boundary. Small differences of the *apparent* Fermi wave vectors in the different experimental reports could be attributed to slightly different defect levels. They may also be caused by the finite band dispersion perpendicular to the wires (Ahn *et al.*, 2005): Fermi level crossings appear at slightly different values of k_{\parallel} , depending on the value of k_{\perp} in these data. In spite of the different spin quantum numbers of the two parabolic branches, the observation that the band gap openings only occur at the 1×2 zone boundaries hints at the significance of electron-lattice (or spin-lattice) coupling in these metal-insulator transitions.

4. Defects and interchain correlations

Defects and interchain correlations in quasi-1D systems have a critical effect on their properties. They can affect the CDW transition temperature, limit correlation lengths, pin CDW fluctuations, and alter the effective dimensionality of the system, and a careful analysis of their role is necessary to understand the mechanisms of the CDW formation in these quasi-1D atom wires.

As mentioned in Sec. I, the observation of a phase transition at finite temperature requires some coupling between the atom wires or between the atom wires and the substrate. This coupling suppresses the thermodynamic fluctuations that otherwise would destroy long-range order in one dimension. However, LEED (Lipton-Duffin *et al.*, 2006) and STM (Losio *et al.*, 2001; Sauter *et al.*, 2007) data of Si(557)-Au showed that the $\times 2$ ordering of the Si adatom wires at RT and the $\times 2$ ordering of the step-edge wires at low temperature are not laterally correlated. The same is true for the $\times 3$ and $\times 2$ periodicities in neighboring wires on Si(553)-Au; their phases appear to be random according to both STM and LEED (Ahn *et al.*, 2005; Snijders *et al.*, 2006) (see Fig. 13). These results indicate an almost negligible 2D coupling in the atom wire arrays, consistent with the extremely small (but finite) 2D coupling inferred from the ARPES experiments (cf. Secs. II.B.1 and II.C.1). However, the absence of large interchain interaction apparent in STM images may well be related to the ubiquitous defects at the Si(557)-Au and Si(553)-Au surfaces. If the boundary conditions imposed by these defects on the *phase* of the CDW are stronger than the interchain coupling, a random distribution of defects will destroy long-range 2D order. STM images indeed suggest that the vacancylike defects in neighboring step-edge wires on Si(557)-Au are uncorrelated: at RT the position of two neighboring vacancylike defects in the step-edge wire can be both in phase or out of phase with respect to a $\times 2$ lattice (Yeom *et al.*, 2005). This results in the apparent absence of phase correlations between the neighboring atom wires on Si(557)-Au. Note that even at room temperature STM images sometimes reveal faint CDW periodicities

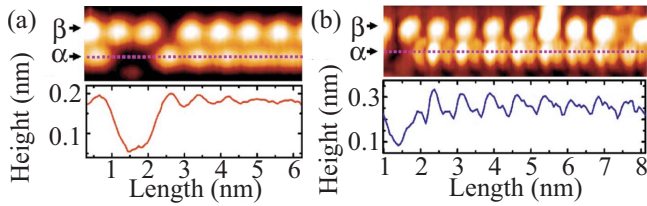


FIG. 15. (Color online) Empty state STM image and line profile of the Si(557)-Au surface near a defect in the step-edge Si wire at (a) room temperature and (b) 78 K. From [Yeom *et al.*, 2005](#).

whose phase is locked in by the defects. For example, step-edge wires on Si(557)-Au exhibit a clear $\times 2$ periodicity at room temperature ([Yeom *et al.*, 2005](#); [Sauter *et al.*, 2007](#)) [see Fig. 15(a)]. [Yeom *et al.* \(2005\)](#) showed that the presence of vacancylike defects in the step-edge wire induces a *local* phase-locked $\times 2$ corrugation that slowly decays along the wire direction.

STM images of the Si(553)-Au surface in [Snijders *et al.* \(2006\)](#) also indicate that the phase correlation between the low-temperature $\times 3$ periodicities in neighboring atom wires is very weak. However, for long wire segments (i.e., low defect concentrations), one frequently observes a sequence of phase slips consisting of a single $\times 4$ period in neighboring wire segments that are somehow correlated. The individual segments have the low-temperature $\times 3$ periodicity but the phase slips do not arise from a misfit between the $\times 3$ periodicity and defect locations. This suggests that the interchain coupling is non-negligible and becomes apparent when the defect concentration is below a critical level. In addition, the observation of STM-induced movement of defects indicates that it must be possible to fabricate wire lengths of, e.g., ten lattice spacings that should exhibit misfit-induced phase slips. These phase slips carry a fractional charge and spin, and this system thus allows for a controlled study of fractional quantum numbers in a quasi-1D system ([Snijders *et al.*, 2006](#)).

One of the open questions regarding the exact phase-transition mechanism in these atom wire systems and the influence of defects on this mechanism is whether or not the local charge corrugations observed near defects in the STM images are indicative of a defect-mediated condensation mechanism, possibly implying an increase of the CDW gap and transition temperature [cf. [McMillan \(1975\)](#), [Weitering *et al.*, \(1999\)](#), and [Snijders *et al.* \(2006\)](#)]. Defects are known to stabilize local CDW domains ([McMillan, 1975](#)). Order-disorder CDW transitions such as the $c(4\times 2)$ -to- 2×1 transition on Si(100) also indicate the pinning of low-temperature $c(4\times 2)$ domains near defects on the surface ([Hamers *et al.*, 1986](#)). In spite of the many similarities between Si(553)-Au and Si(557)-Au, these systems seem to behave differently in this context. In the case of Si(557)-Au, the $\times 2$ corrugation near defects observed at room temperature appears to be different from the $\times 2$ corrugation of the CDW phase below T_c [see Fig. 15(b)]. This suggests that these charge or lattice corrugations have different origins

([Yeom *et al.*, 2005](#)). Step-edge defects also alter the $\times 2$ CDW corrugation below the transition temperature ([Yeom *et al.*, 2005](#)). Different $\times 2$ configurations thus seem to compete in the vicinity of defects. For Si(557)-Au there is thus no evidence that the presence of defects increases the CDW transition temperature of the atom wires. The different appearances of the $\times 2$ periodicities near defects at room temperature and the $\times 2$ periodicity of the low-temperature condensate seem to rule out the picture of the CDW as a spatially extended Friedel oscillation, even though the corrugation in filled and empty state STM images appears to be out of phase ([Krawiec *et al.*, 2006](#)), as for ordinary CDWs.

In contrast, the Si(553)-Au surface does seem to show a defect-induced increase of the CDW transition temperature. [Crain and Pierce \(2005\)](#) performed a detailed spatially resolved STS experiment at room temperature on step-edge wire segments that were cut short by defects. Their results indicated a charge transfer from the interior of the wires to the (two) end atoms or zero-dimensional “end states.” [Snijders *et al.* \(2006\)](#) later indicated that the corrugation of the atom wires near defects is very similar to the corrugation of the low-temperature $\times 3$ CDW phase. Evidently, the CDW already manifests itself at room temperature at the ends of the wire segments with a charge-density maximum being located next to a defect. As the temperature decreases, this CDW gradually extends to the full length of the wire segment (see Sec. II.C.2 and Fig. 13) ([Snijders *et al.*, 2006](#)). Note that at room temperature the spatial extent of the defect-induced CDW is considerably smaller for Si(553)-Au (≤ 1 unit cell) than for Si(557)-Au (~ 4 unit cells), indicating that the perturbations by defects play out differently.

Although the effect of these atomic defects is local in nature, the mesoscopic properties of these systems are affected as well. The atom wires on Si(557)-Au reveal insulating behavior in surface conductivity measurements between 150 and 300 K [see Fig. 16(b)] ([Schöck *et al.*, 2003](#); [Okino *et al.*, 2004, 2007](#)). Even though this result seems to be in conflict with the observation of a metallic surface in STS and ARPES experiments above the CDW transition temperature (cf. Sec. II.B.1), these measurements can be reconciled by the observed presence of defects in the atom wires, which effectively cut the wires into small segments [see Fig. 16(b)]. This leads to activated carrier hopping between wire segments with an energy barrier of 55 meV ([Okino *et al.*, 2004](#)). [Okino *et al.* \(2007\)](#) also performed surface sensitive transport experiments on Si(553)-Au [see Fig. 16(a)]. In contrast to Si(557)-Au, these experiments revealed a metallic surface at high temperatures and a clear metal-insulator transition at 160 K. It was suggested that the larger 2D coupling of the atom wires on Si(553)-Au as compared to Si(557)-Au allows the carriers to hop more easily across the wires. Even though defects cut the atom wires into small segments, the 2D coupling evidently leads to a metallic percolation path.

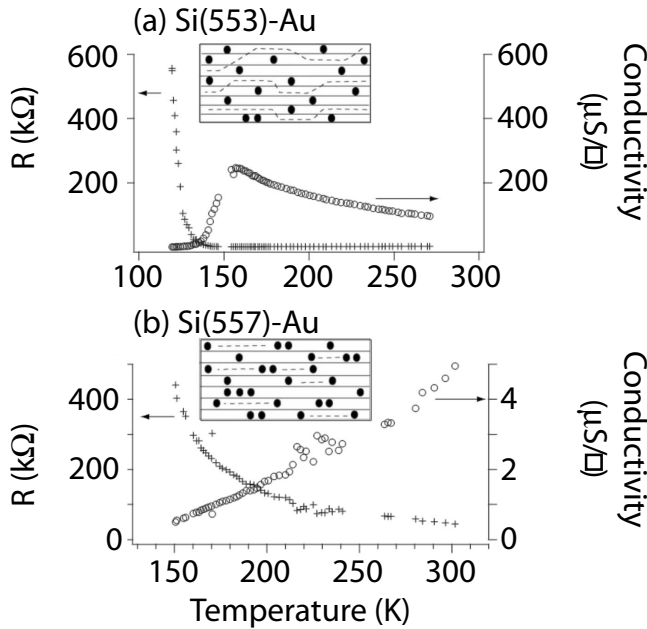


FIG. 16. Temperature-dependent resistance and conductivity of the (a) Si(553)-Au and (b) Si(557)-Au surface states, revealing a metal-insulator transition in the former, whereas the latter shows insulating behavior over the full temperature range. The insets show the room-temperature transport paths (dashed) in relation to the defects (dots) present on the surfaces. Adapted from Okino *et al.*, 2007.

III. In ATOM WIRES ON Si(111)

A. In/Si(111)

Indium atom wires on Si(111) also form a triple-band system undergoing a Peierls-like distortion at low temperatures. This electronic instability may seem easier to interpret than those in the Au-induced reconstructions on high index Si surfaces because the structures are simpler and better understood, their Fermi contours have also been mapped with great accuracy, and above all the surfaces are much better ordered. There are far fewer (and only extrinsic) defects than on the Au-induced reconstructions and their role in the phase transition may only be of secondary importance. We first discuss the nature of the phase transition and its driving force. Atomistic details of this phase transition will be discussed in Sec. III.A.4.

1. Atomic and electronic structure

Indium adsorption on Si(111) produces a wide variety of surface reconstructions (Lander and Morrison, 1965). Among these reconstructions, the 4×1 phase observed at room temperature appears to be unique in that it is quasi-1D in nature, breaking the threefold rotational symmetry of the substrate. Early STM studies by Nogami *et al.* (1987, 1988) showed that the 4×1 structure consists of ridges that are running parallel to the three symmetry equivalent $[110]$ directions of the Si substrate, thus producing three domains on the surface. It has now been firmly established by surface XRD (Bunk

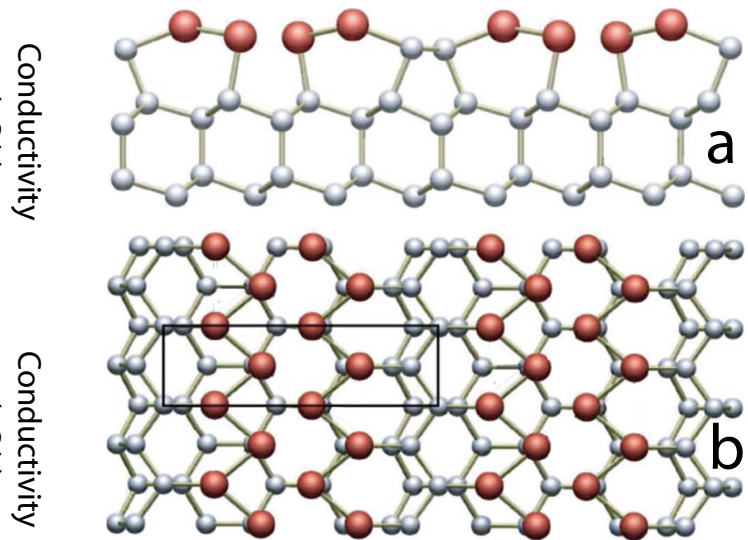


FIG. 17. (Color online) Structural model of the Si(111)- 4×1 -In reconstruction. (a) Side and (b) top view. Large circles are the In atoms forming parallel zigzag wires along the $[110]$ direction. The 4×1 unit cell is indicated. Adapted from Stekolnikov *et al.*, 2007.

et al., 1999; Kumpf *et al.*, 2000), LEED (Mizuno *et al.*, 2003; Wang *et al.*, 2005), and first-principles total energy calculations (Cho *et al.*, 2001, 2005; Wang *et al.*, 2003; González *et al.*, 2005, 2006b; Tsay, 2005; Lopez-Lozano *et al.*, 2006; Cho and Lee, 2007; Stekolnikov *et al.*, 2007) that these ridges consist of two parallel zigzag wires of In atoms. The zigzag wires are separated by single wires of Si atoms (Fig. 17), implying an absolute coverage of one In atom per Si surface atom (Lee *et al.*, 2003).

In spite of the fact that the total number of valence electrons per 4×1 unit cell is even, the system is clearly metallic at room temperature, as indicated by photoemission (Abukawa *et al.*, 1995; Yeom *et al.*, 1999; Ahn, Byun, *et al.*, 2004; Ahn *et al.*, 2007; Sun *et al.*, 2008), inverse photoemission (Hill and McLean, 1999), STM (Kraft *et al.*, 1997; Park *et al.*, 2004; Lee *et al.*, 2005; González *et al.*, 2009) and EELS (Sakamoto *et al.*, 2000; Hwang *et al.*, 2007; Liu *et al.*, 2008). This indicates the presence of multiple surface-state bands. Indeed ARPES experiments (Abukawa *et al.*, 1995; Yeom *et al.*, 1999; Ahn, Byun, *et al.*, 2004; Ahn *et al.*, 2007) at room temperature reveal three quasi-1D metallic bands in the fundamental band gap of the bulk Si substrate. Accordingly, the system has been described as a triple-band Peierls system, similar to the case of Si(553)-Au. The surface-state bands are commonly denoted as the m_1 , m_2 , and m_3 bands and disperse almost parabolically along the wire direction (Fig. 18). The band minima are all located at the X point of the surface Brillouin zone. The bands cross E_F at parallel momentum values of 0.75, 0.54, and 0.41 \AA^{-1} , respectively, as measured from the zone center for zero perpendicular momentum (Ahn, Byun, *et al.*, 2004). When integrated over the first Brillouin zone, one obtains band fillings of 0.11 (m_1), 0.38 (m_2), and 0.50 (m_3) (Ahn, Byun, *et al.*, 2004). This band

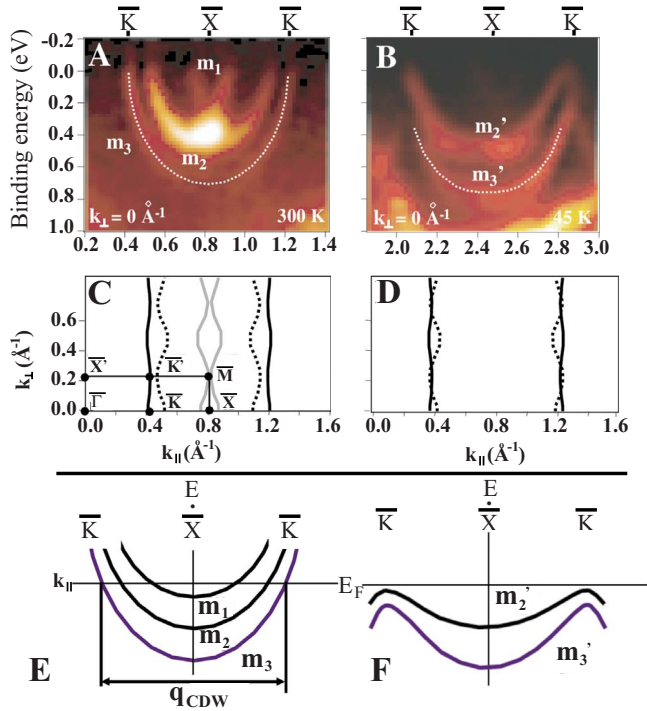


FIG. 18. (Color online) ARPES band dispersions of the 4×1 [(a) 300 K] and 8×2 [(b) 45 K] phases, recorded along the In wire direction. Surface Brillouin zone and schematic of the experimentally determined Fermi contours at (c) 300 K and (d) 45 K. Schematic illustrations of the surface-state band structure at (e) 300 K and (f) 45 K. Adapted from [Ahn, Byun, et al., 2004](#).

structure is nicely captured by the various DFT calculations ([Cho et al., 2001, 2005](#); [Wang et al., 2003](#); [González et al., 2005, 2006b](#); [Tsay, 2005](#); [López-Lozano et al., 2006](#); [Cho and Lee, 2007](#); [Stekolnikov et al., 2007](#)) for the structure model by [Bunk et al. \(1999\)](#). Figure 18 shows the experimentally determined Fermi contours of all three bands ([Ahn, Byun, et al., 2004](#)). The small wiggling of the Fermi contours, most notably for the m_1 band, indicates a weak coupling in the direction normal to the In atom wires, similar to the Au/Si atom wires. The anisotropy of the band structure can be quantified by the ratio of the transfer integrals t_{\parallel}/t_{\perp} , which amounts to 72 for the m_3 band and about 8 for the other two bands ([Ahn, Byun, et al., 2004](#)). Contour m_3 thus appears to be almost perfectly 1D and also seems to be perfectly nested for a $\times 2$ Peierls instability, as would be expected for a half-filled band. Indeed, the system undergoes a phase transition at lower temperatures as discussed in the following sections.

2. Metal-insulator transition

The 4×1 arrangement of the In atom wires initially transforms into a 4×2 structure at 120 K, which upon further cooling gradually converts into a 8×2 structure. This reversible phase transition was first reported by [Yeom et al. \(1999\)](#) who characterized this transition with ARPES, STM, and reflection high-energy electron dif-

fraction. The phase transition was attributed to a CDW instability induced by the “perfect nesting” of the half-filled m_3 band, thus producing the observed period doubling along the wire direction. The CDW ground state was found to be insulating with a (half-)gap at the zone boundary of the order of 50–100 meV. Later ARPES studies unveiled the backfolding of the m_2 and m_3 bands (henceforth labeled as the m_2' and m_3' bands) around the K point, which is located halfway through the 4×1 Brillouin zone ([Ahn, Byun, et al., 2004](#); [Sun et al., 2008](#)). Surprisingly, the m_1 band disappears completely below 120 K indicating that it is pushed above E_F . This implies a charge transfer from m_1 to the m_2 surface-state band (leaving the m_3 band exactly half filled). Note that this resembles the charge transfer between the down step-edge band and the Si-Au bands described in Sec. II.B.3. Within the Peierls picture, the stabilization of the low-temperature phase in the In/Si system should be attributed primarily to the 0.34 eV gap in the m_3' band at the K point.⁷

The structure of the CDW condensate is still subject to intense debate. XRD studies indicate that the period doubling is associated with the pairing of In atoms at the outer ridges of the double zigzag wires ([Kumpf et al., 2000](#)). This results in the formation of In trimers and a period doubling along the wire direction, which accounts for the existence of a 4×2 structure. The true ground state is an 8×2 structure, which can be constructed by “out-of-phase” arrangements of In trimers in neighboring In wires (Fig. 19). Note that there should be two different 8×2 structures, depending on the layout of 4×2 subcells, which appears to be corroborated by STM experiments ([Guo et al., 2005](#)).

3. Order-parameter fluctuations

Variable-temperature STM is a powerful tool for investigating the atomistic details of phase transitions at surfaces ([Weitering et al., 1999](#)). [Park et al. \(2004, 2005\)](#), [Guo et al. \(2005\)](#), [Lee et al. \(2005\)](#), and [Lee \(2006\)](#) studied the phase-transition dynamics and the role of defects in the transition in close vicinity to T_c . Their observations all seem consistent: 1D stripes of the low-temperature 4×2 phase or “charge-order fluctuations” are seen to nucleate near T_c . In defect-free regions, these 1D domains produce a dark image contrast (compared to the surrounding metallic 4×1 phase), consistent with the opening of a (pseudo)gap ([Guo et al., 2005](#); [Lee et al., 2005](#); [Park et al., 2005](#)). Spectroscopically, these 1D charge-ordered stripes are indistinguishable from the low-temperature 8×2 phase, meaning that their I - V curves in STS are identical. The $\times 2$ ordering within the stripes fades at higher temperature ([Guo et](#)

⁷Note that other investigations by ARPES ([Gallus et al., 2001](#); [Yeom et al., 2002](#)), STS ([Guo et al., 2005](#); [Lee et al., 2005](#)), and EELS ([Sakamoto et al., 2000](#)) indicate the existence of a “pseudogap” as opposed to a real gap.

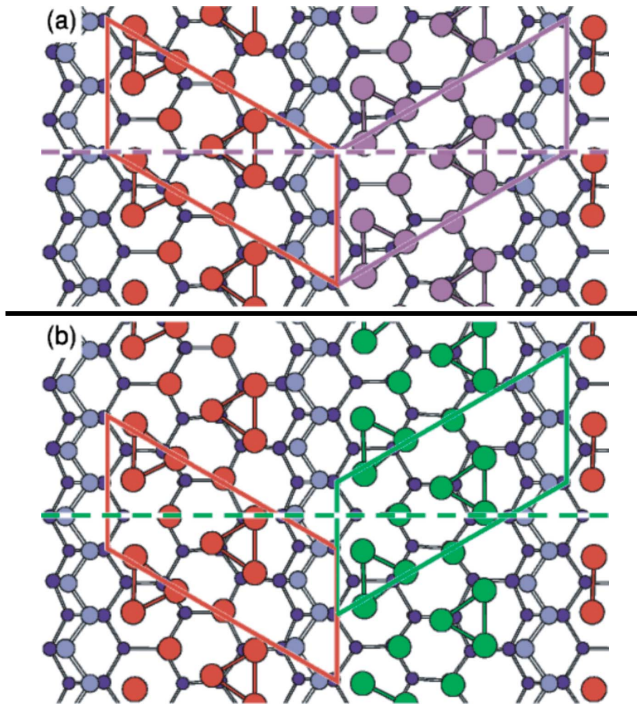


FIG. 19. (Color online) Trimer model for the low-temperature 8×2 structure. There are two degenerate 8×2 structures, arising from the two possible arrangements of In trimers. This is best seen from the registry shift of the 4×2 subcells that are indicated in (a) and (b). The 8×2 unit cell and glide plane of the structure are also shown. Adapted from [Kumpf *et al.*, 2000](#).

[al., 2005\) though the stripes remain electronically distinct from the surrounding \$4 \times 1\$ matrix.](#)

These 1D charge-ordered striped domains change with each STM scan ([Guo *et al.*, 2005](#); [Lee *et al.*, 2005](#); [Park *et al.*, 2005](#)). Some stripes stay at their location but change their lengths while others appear and disappear abruptly. This chaotic appearance and disappearance pattern was attributed to fluctuating CDWs ([Guo *et al.*, 2005](#); [Lee *et al.*, 2005](#); [Park *et al.*, 2005](#); [Lee, 2006](#)). A different type of $\times 2$ charge-order modulation was seen near defects ([Ahn, Byun, *et al.*, 2004](#); [Lee *et al.*, 2004, 2005](#); [Lee, 2006](#)). These charge-ordered stripes are quasi-stationary in the sense that they are visible in each scan but their lengths do fluctuate between successive scans. Their apparent brightness in the STM images is similar to that of the surrounding 4×1 phase. It has been concluded that these structures are metallic and must therefore be different from the low-temperature charge-ordered phase.

When the surface is cooled through the phase transition, the 1D charge-ordered domains coalesce into the low-temperature 8×2 phase ([Guo *et al.*, 2005](#); [Lee *et al.*, 2005](#); [Park *et al.*, 2005](#); [Lee, 2006](#)). The 4×1 and 8×2 phases coexist over a rather wide temperature range of about 40 K. The sequential STM images in Fig. 20, which were recorded slightly below T_c ([Park *et al.*, 2005](#)), show that large metallic 4×1 domains abruptly convert into 8×2 charge-ordered regions. This process could be triggered by a minute change of the temperature or a

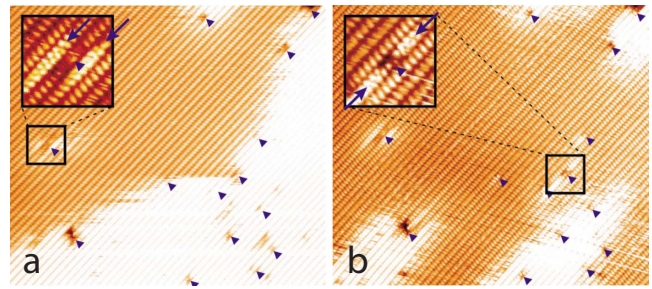


FIG. 20. (Color online) Domain fluctuations in the Si(111)- 4×1 -In reconstructions. (a) and (b) Sequential $60 \times 60 \text{ nm}^2$ STM images showing $4 \times 1 \rightarrow 8 \times 2$ domain fluctuations at 123 K. Defects are indicated by arrowheads. The insets are close-up views of defects which locally induce a 4×2 structure. From [Park *et al.*, 2005](#).

perturbation by the STM tip or it could be a manifestation of intrinsic order-parameter fluctuations. Because of this abruptness of the transition, [Park *et al.* \(2005\)](#) concluded that the phase transition must be of first order and proceeds via a domain-by-domain conversion at the nanoscale. The definition of the domains and their local transition temperatures seems to be correlated with the distribution of defects. [Lee *et al.* \(2005\)](#) pointed out, however, that such nanoscale inhomogeneity near T_c is typical of second-order phase transitions. Because thermodynamic quantities such as the long-range order parameter are macroscopic averaged quantities, abrupt changes at the nanoscale are not contradictory to the notion of a continuous second-order phase transition.

Upon further lowering of the temperature, the surface becomes predominantly 8×2 . One occasionally finds 1D 4×1 metallic stripes that are embedded in the 8×2 matrix ([Lee *et al.*, 2005](#)). These 1D segments also exhibit fluctuations as they change their length with successive STM scans. These length changes imply concerted shifts of the $\times 2$ features in the neighboring charge-ordered domains since the $\times 8$ interchain ordering surrounding these metallic stripes always seems preserved ([Lee *et al.*, 2005](#)). These observations are best summarized by the phase diagram of [Guo *et al.* \(2005\)](#) in Fig. 21. In this phase diagram, the structural order parameter $P_{\times 2}$ is defined as the area fraction (or percentage) of the $\times 2$ domains (including the 2D 4×2 and 8×2 domains and the 1D charge-ordered stripes) averaged over a number of large-scale STM images. The onset of the structural transition occurs near 145 K. Between 135 and 145 K, the system is characterized by the nucleation of 1D charge-ordered stripes embedded in the 2D 4×1 phase. Two-dimensional 4×1 and 8×2 domains coexist between 105 and 135 K. The 4×1 to 8×2 structural transition is completed at 85 K although the shape and size of the two degenerate 8×2 domains keep evolving at low temperature. [Guo *et al.* \(2005\)](#) also defined an “electronic order parameter” P_{SM} , which is defined as the area fraction of the “low brightness” domains or domains with the nonmetallic image contrast. The electronic phase transition seems to be complete at 105 K.

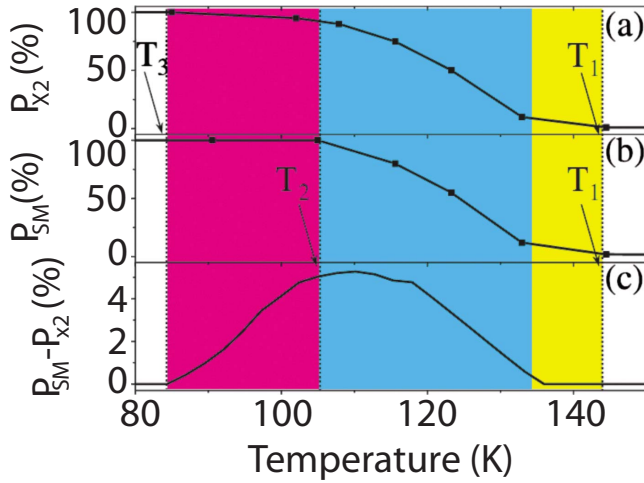


FIG. 21. (Color online) Order parameters (a) $P_{\times 2}$ (b) P_{SM} , and (c) their difference in the vicinity of T_c . Adapted from Guo *et al.*, 2005.

The difference between the structural and electronic order parameters produces a small hump of order 5%, which was shown to correspond to a 4×1 nanophase domain with a nonmetallic instead of a metallic contrast. The existence of these novel nanophase domains is indicated by the line scan in the STM image in Fig. 22. (Guo *et al.*, 2005). The line profile along AB shows that the apparent height of the three 4×1 wires on the right is identical to the 4×2 wire in the middle and lower than that of the metallic 4×1 wires on the left.

4. Alternative model of the transition

There are still serious problems with the Peierls picture. First, DFT total energy calculations that would seem to corroborate trimer formation (Cho *et al.*, 2001, 2005; Wang *et al.*, 2003; López-Lozano *et al.*, 2006) cannot reproduce the nonmetallic ground state indicated by the most detailed ARPES experiments (Ahn, Byun, *et al.*, 2004; Sun *et al.*, 2008). Specifically, the theoretical $m1$ band always crosses E_F in the 4×2 state, and STM image simulations for the 4×2 structure required an arti-

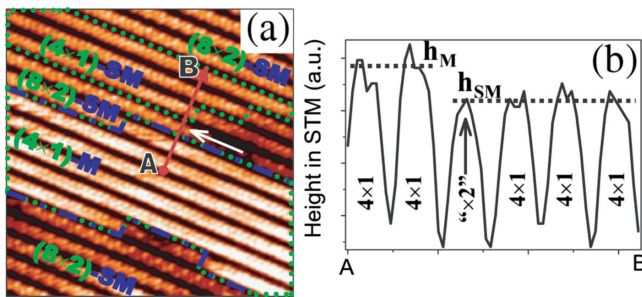


FIG. 22. (Color online) Nanophase domains in $\text{Si}(111)\text{-}4 \times 1\text{-In}$. (a) STM image of the $\text{In}/\text{Si}(111)$ interface at 110 K. The electronic metal-insulator contrast (bright-dark domains) is separated by dashed lines. The 4×1 domains are marked with dotted lines out of the 8×2 areas. (b) The line profile along AB . From Guo *et al.*, 2005.

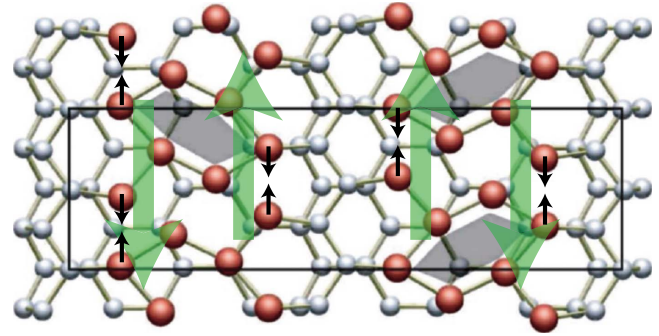


FIG. 23. (Color online) Hexagon model for the low-temperature 4×2 and 8×2 structures, showing the displacement patterns for both shear distortion and dimerization. Adapted from Stekolnikov *et al.*, 2007.

ficial shift of the Fermi level to resemble experimental images because the experimental system is nonmetallic (Cho *et al.*, 2005). Second, the observed Peierls gap by ARPES can only be a fraction of the total band gap. This suggests that the gap is of the order of 100 meV or more, which seems extremely high in light of the T_c of 120 K in weak-coupling BCS theory.⁸

Recent theoretical studies (González *et al.*, 2005, 2006b; Stekolnikov *et al.*, 2007) indicated that the Peierls-type dimerization of the outermost In atoms is accompanied by a shear distortion, whereby neighboring zigzag wires are displaced in opposite directions. This mechanism leads to the formation of In hexagons rather than trimers, produces a 4×2 periodicity, and fully opens a band gap (Fig. 23). The 8×2 structure can subsequently be obtained by alternating the hexagon orientation and arises from interchain coupling. The energy cost of the shear distortion is very low, which allows the system to fluctuate chaotically between four degenerate 4×2 ground states. Above 120 K, these fluctuations produce an average 4×1 structure on the time scale of STM. While this picture does involve the dimerization or Peierls distortion in the outer atom rows, the insulator-metal transition is fundamentally different from a CDW mechanism driven by Fermi surface nesting. Instead, the transition at 120 K would be driven by a soft shear phonon and could be characterized as an order-disorder transition, akin to the $c(4 \times 2) \rightarrow 2 \times 1$ transition induced by fluctuating dimers on $\text{Si}(100)$ (Wiekliem *et al.*, 1990) or the dynamical fluctuations of Sn adatoms on the $\text{Ge}(111)\text{-}\sqrt{3} \times \sqrt{3}\text{-Sn}$ surface (Avila *et al.*, 1999; Pérez *et al.*, 2001) and incompatible with the traditional CDW characterization of weak- and strong-coupling regimes.

The stability of the In hexagon arrangement was challenged by Cho and Lee (2007) who claimed that the structure by González *et al.* (2005, 2006b) was not fully

⁸This picture can possibly be salvaged by recognizing that thermodynamic fluctuations can lower the transition temperatures well below the mean-field theory prediction (Yeom *et al.*, 1999; Lee *et al.*, 2005).

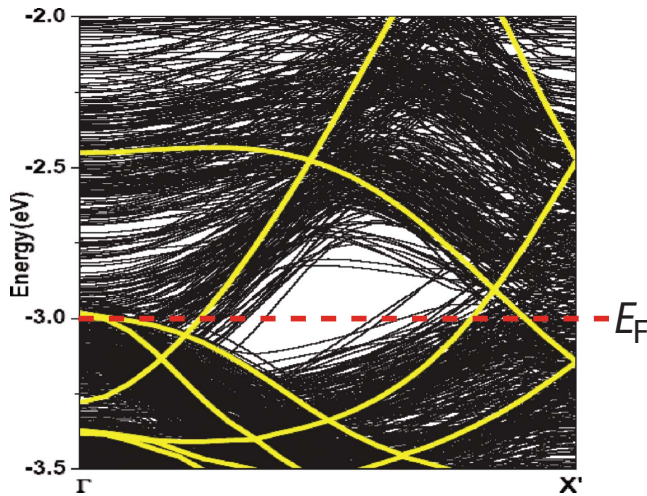


FIG. 24. (Color online) Superimposed electronic band structures for 100 different atomic configurations (one every 500 fs) from molecular dynamics simulations at 450 K. The light lines show the band structure of the ideal (static) 4×1 structure (in a 4×2) unit cell. Adapted from [González et al., 2006b](#).

relaxed. [Stekolnikov et al. \(2007\)](#) also found the 4×2 hexagon structure to be metastable but obtained a stable 8×2 arrangement.⁹ The strongest evidence in favor of the hexagon model is the observation of a nonmetallic ground state. Specifically, in the hexagonal model, the $m1$ surface-state band is shifted above E_F while the $m2'$ and $m3'$ bands exhibit gaps at the zone boundary, consistent with the ARPES data ([Ahn, Byun, et al., 2004](#); [Sun et al., 2008](#)).

In photoemission experiments electron bands are measured on a time scale of the order of femtoseconds, which is much shorter than the time scale of the fluctuations. The photoemission spectrum above 120 K should thus consist of a superposition of electronic band structures of all possible intermediate atomic configurations and the experimental observation of distinct surface state bands above 120 K may seem inconsistent with the dynamical fluctuation scenario. Figure 24 plots instantaneous band structures that were calculated with 500 fs intervals ([González et al., 2006b](#)). These snapshots of the electronic structure were obtained from molecular dynamics simulations assuming a surface temperature $T = 450$ K. In general, intermediate configurations that are close to the 4×2 ground state are semiconducting whereas configurations farther away are often metallic. The system thus exhibits metal-semiconductor fluctuations that are associated with the dynamical structural fluctuations. It is now possible to identify envelopes of bands that closely resemble the distinct bands of the 4

$\times 1$ surface. Whether or not such a broadening or mix-up of the bands should have been observable in the experimental data still remains a matter of dispute ([González et al., 2006a](#); [Yeom, 2006](#)).

More direct support for the dynamical fluctuation model comes from the detailed STM and STS investigations in [González et al. \(2009\)](#). Here it is shown that extensive STM image simulations for the hexagon structure, using the nonequilibrium Green-Keldysh formalism ([Snijders et al., 2005](#)), agree well with experimental STM images at different biases, recorded at 42 K. STS spectra indicate that the band gap of the 4×2 and 8×2 domains is 0.3 eV and independent of temperature down to 40 K. This suggests that the insulator-metal transition (at 120 K) is very abrupt, unlike a CDW scenario where the gap is expected to follow the temperature dependence of the BCS gap equation. This abruptness was also observed in ARPES ([Sun et al., 2008](#)) and surface transport measurements ([Uchihashi and Ramspurger, 2002](#); [Tanikawa et al., 2004](#)). Note that the 0.3 eV band gap is in excellent agreement with surface transport measurements ([Tanikawa et al., 2004](#)).

By varying the STS set point or tip-sample distance, it was furthermore concluded ([González et al., 2009](#)) that the tunneling current arises mostly from states near Γ in the surface Brillouin zone. The sudden collapse of the gap at 120 K seen in STS was therefore attributed to the appearance of the $m1$ electron pocket near Γ . In ARPES, the $m1$ pocket appears at the 4×1 zone boundary or X point but this X point is symmetry equivalent with the Γ point of the fluctuating 4×2 structure. ARPES and STS are thus fully consistent within the dynamical fluctuation picture. The metallic I - V spectra above 120 K could be fitted assuming a half-Gaussian distribution of gaps, centered at E_F ([González et al., 2009](#)). Similar gap distributions were obtained from 500 fs spaced snapshots of the band structure in first-principles molecular dynamics simulations ([González et al., 2006b](#)).

Finally, the 40 meV gap at the zone boundary observed by ARPES below 120 K ([Ahn, Byun, et al., 2004](#)) is much smaller than the 0.3 eV STS gap near Γ ([González et al., 2009](#)). It is important to realize, however, that ARPES measurements do not reveal the true gap because ARPES only probes the filled states. Molecular dynamics simulations indicate that the Peierls gap at X persists above E_F even at 200 K, consistent with the proposition that the (fluctuating) 4×2 structure and hence the Peierls dimerization also persist. This is to be expected from the BCS gap relation, which predicts a Peierls temperature of ~ 1000 K for a 0.3 eV gap. The downward shift of the $m1$ electron pocket thus appears to be most relevant for the insulator-metal transition at 120 K. The shift of $m1$ is associated with the excitation of a shear phonon and not with Fermi surface nesting ([González et al., 2006b](#)). In this scenario, the transition should clearly be of the order-disorder type as opposed to a displacive CDW transition. The evolution of the order parameter and specifically the abruptness of the

⁹Note that the formation energies of the various structure models differ marginally, meaning that the ground-state structure obtained from these calculations depends on the used approximations to the exchange-correlation potential (i.e., local-density approximation versus generalized gradient approximation) and treatment of the d electrons.

phase transition indeed seem to be better captured by a 2D Ising model (Yagi and Yoshimori, 2005; Yagi *et al.*, 2007, 2008) as opposed to the BCS theory for CDWs.

The dynamical fluctuation scenario of González *et al.* (2006b) seems consistent with the observation of a non-metallic 4×1 phase (see Fig. 22 and Sec. III.A.3) (Guo *et al.*, 2005). As the rapid fluctuations between the four degenerate 4×2 structures slow down with decreasing temperature, the system will develop an intermediate insulating 4×1 wire. Once the intrachain $\times 2$ fluctuations completely freeze out, charge ordering within isolated wires becomes observable. Finally, the 8×2 reconstruction develops as the temperature is lowered even further due to antiferromagnetic interactions between the 4×2 wires (González *et al.*, 2006b). All these structures, such as the insulating 4×1 wires, individual 4×2 wires, and the 2D 4×1 and 8×2 phases, have been observed in experiment (Guo *et al.*, 2005).

5. Possible evidence of non-Fermi-liquid behavior

The possibility of non-Fermi-liquid-like properties of the metallic 4×1 wires above the Peierls transition was explored by measuring the energy and width of the intraband plasmon excitations using EELS (Hwang *et al.*, 2007; Liu *et al.*, 2008). A series of EELS spectra by Liu *et al.* (2008) as a function of momentum transfer showed a dispersive loss feature along the In wire direction. No such feature is seen in the direction normal to the In wires and it is also absent below the metal-insulator transition. This indicates that the loss feature should be identified as a quasi-1D metallic plasmon excitation. The momentum dispersion is shown in Fig. 25.¹⁰ The best theoretical fit to the data was obtained by assuming a parallel wire system with an interwire distance of 13.3 Å using a nonlocal dielectric response theory with self-consistent local field corrections. A similar analysis on the Si(557)-Au system indicated the increased importance of dynamical exchange-correlation effects in 1D systems, leading to a significant redshift of the plasmon frequency at nonzero parallel momentum (Nagao *et al.*, 2006). Hwang *et al.* (2007) pointed out that the momentum dependence of the *linewidth* of the plasmon (i.e., its lifetime) is a strong indicator of non-Fermi-liquid behavior even though possible spin-charge separation must be very small in this system. Interestingly, the plasmon dispersion can only be fitted to the m_3 surface-state band (Liu *et al.*, 2008). The absence of plasmonic excitations in the EEL spectra for the m_1 and m_2 surface-state bands is not yet understood.

6. Role of defects

An important issue in the literature on charge ordering is whether the charge-ordering transition nucleates

¹⁰Note that a pure 1D metallic plasmon should exhibit a linear dispersion. The observed nonlinear dispersion is explained by the finite transverse coupling between the In atom wires (Nagao *et al.*, 2006; Liu *et al.*, 2008).

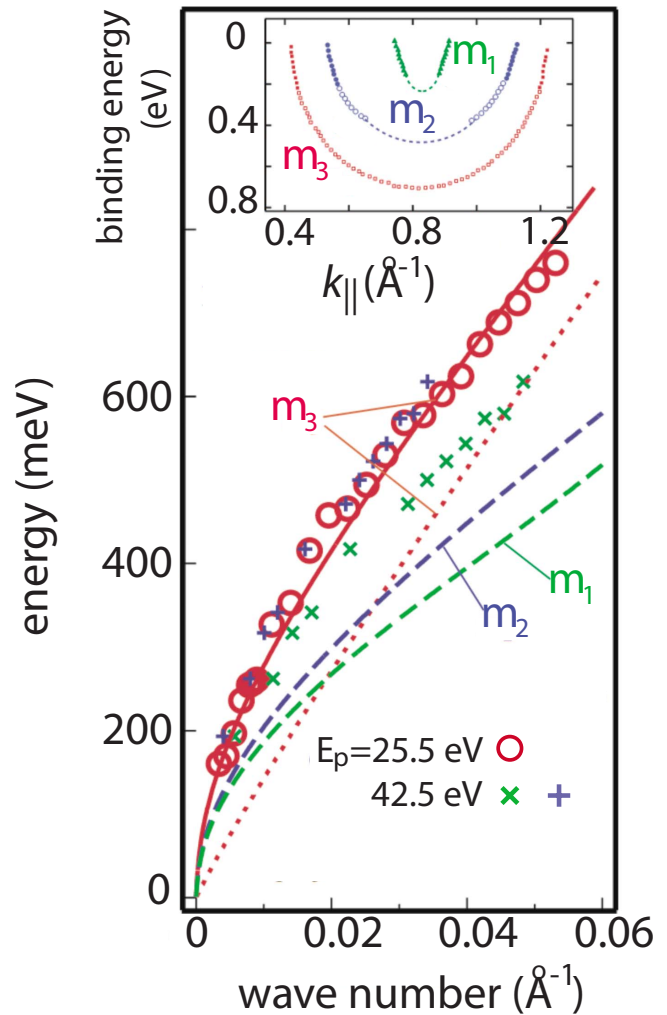


FIG. 25. (Color online) 1D plasmon dispersion. Open circles are experimental data parallel to the wire direction; crosses (\times) are data recorded at a 45° angle and the pluses ($+$) are their projection onto the wire direction. The solid and dashed lines are the calculated plasmon dispersions for the m_1 , m_2 , and m_3 surface-state bands (shown in the inset) based on a parallel multiwire model. The straight dotted line is the calculated plasmon dispersion of an isolated metallic wire. Adapted from Liu *et al.*, 2008.

at defects (Weitering *et al.*, 1999; Melechko *et al.*, 2000; Snijders *et al.*, 2006). As mentioned in Sec. III.A.3, defects do induce a local $\times 2$ ordering above T_c but this $\times 2$ structure seems to be different from the low-temperature phase and is less susceptible to fluctuations. Furthermore, because 1D charge-ordered stripes are seen to nucleate in defect-free regions, there is no clear evidence that these defects play a crucial role in the onset of charge-ordering transition. On the other hand, defects seem to inhibit the condensation of the low-temperature 8×2 phase below T_c . This is shown in Fig. 20 where the metallic domains bounded by defects seem to persist at 123 K while those in defect-free regions are easily converted into charge-ordered domains (Park *et al.*, 2004; Lee, 2006). A possible explanation is that the random site location of the defects hinders the trans-

verse ordering in the low-temperature phase (Lee, 2006). In addition, even when the phase transition is almost completed at an even lower temperature, the $\times 2$ charge ordering is still suppressed in short wire segments between vacancy defects if the vacancy spacing (or length of the wire segment) corresponds to an odd multiple of the Si lattice constant (Park *et al.*, 2004). In this case, the disorder is purely 1D and is not correlated with the neighboring In wires. The out-of-phase site location of the vacancies thus inhibits 1D charge ordering along the wire direction, although the gap opening in the wire segment seems to be complete.

In summary, defects suppress the fluctuations of the 1D charge-ordered stripes above T_c but they do not play a significant role in the onset of the transition, at least not in the case of well-ordered surfaces with relatively few defects. However, they do suppress both 1D and 2D charge ordering below T_c .

IV. CONCLUDING REMARKS

The beauty of these self-assembled atom wire systems is that they represent the “ultimate” or smallest nanowires. They are easily accessible with surface analytical tools such as high-resolution ARPES and STM so that the CDW transition can be explored both in real space and in momentum space with the highest possible resolution. On the theory side, first-principles molecular dynamics simulations have become increasingly accurate in reproducing experimental observations, providing atomistic details of the CDW phase transition that are complementary and beyond the Ginzburg-Landau and renormalization group theories. While many aspects of these phase transitions appear to be system dependent—not in the least because of the critical role of lattice defects—it is becoming increasingly clear that the traditional classification of CDW transitions on the basis of the electron-phonon coupling strength is too restrictive for these nanoscale systems. In particular, the periodicities of the low-temperature phases appear strictly commensurate and independent of the exact band filling. This raises questions about the generality of Fermi surface nesting as an active cause of these CDWs. In this respect, the possible role of the spin-orbit split bands in both the correlations and the phase transition in the Au-based wire systems remains intriguing.

Because of their easy accessibility via imaging and spectroscopy, self-assembled atom wires on surfaces thus unveil unprecedented details in low-dimensional phase transitions, which calls for renewed theoretical efforts to describe these phase transitions in microscopic terms. Fortunately, other quasi-1D surface-based metallic systems have been discovered recently such as the Au/Si(337), Au/Ge(001), Pt/Ge(001), and Pb/Si(557) systems (Gurlu *et al.*, 2003; Ahn, Byun, *et al.*, 2004; Oncel *et al.*, 2005; Tegenkamp *et al.*, 2005, 2008; Kim *et al.*, 2007; Schäfer *et al.*, 2008). It is expected that more detailed studies of these interfaces will broaden the scope of this research, which may offer new opportunities for

identifying unifying principles governing the structure and stability of atom wires.

ACKNOWLEDGMENTS

This work was sponsored in part by the NSF under Contract No. DMR 06-06485. Part of this work was supported by the Office of Basic Energy Sciences, Division of Materials Sciences and Engineering, U.S. Department of Energy, through the Oak Ridge National Laboratory. Research performed by P.C.S. as a Eugene P. Wigner Fellow and staff member at the Oak Ridge National Laboratory, managed by UT-Battelle, LLC, for the U.S. Department of Energy under Contract No. DE-AC05-00OR22725.

REFERENCES

- Abukawa, T., M. Sasaki, F. Hisamatsu, T. Goto, T. Kinoshita, A. Kakizaki, and S. Kono, 1995, *Surf. Sci.* **325**, 33.
 Ahn, J. R., J. H. Byun, J. K. Kim, and H. W. Yeom, 2007, *Phys. Rev. B* **75**, 033313.
 Ahn, J. R., J. H. Byun, H. Koh, E. Rotenberg, S. D. Kevan, and H. W. Yeom, 2004, *Phys. Rev. Lett.* **93**, 106401.
 Ahn, J. R., P. G. Kang, K. D. Ryang, and H. W. Yeom, 2005, *Phys. Rev. Lett.* **95**, 196402.
 Ahn, J. R., H. W. Yeom, E. S. Cho, and C. Y. Park, 2004, *Phys. Rev. B* **69**, 233311.
 Ahn, J. R., H. W. Yeom, H. S. Yoon, and I.-W. Lyo, 2003, *Phys. Rev. Lett.* **91**, 196403.
 Altmann, K. N., J. N. Crain, A. Kirakosian, J.-L. Lin, D. Y. Petrovykh, F. J. Himpsel, and R. Losio, 2001, *Phys. Rev. B* **64**, 035406.
 Aruga, T., 2002, *J. Phys.: Condens. Matter* **14**, 8393.
 Aruga, T., 2006, *Surf. Sci. Rep.* **61**, 283.
 Avila, J., A. Mascaraque, E. G. Michel, M. C. Asensio, G. LeLay, J. Ortega, R. Perez, and F. Flores, 1999, *Phys. Rev. Lett.* **82**, 442.
 Bardeen, J., L. N. Cooper, and J. R. Schrieffer, 1957, *Phys. Rev.* **108**, 1175.
 Barke, I., F. Zheng, T. K. Rügheimer, and F. J. Himpsel, 2006, *Phys. Rev. Lett.* **97**, 226405.
 Bunk, O., G. Falkenberg, J. H. Zeysing, L. Lottermoser, R. L. Johnson, M. Nielsen, F. Berg-Rasmussen, J. Baker, and R. Feidenhans'l, 1999, *Phys. Rev. B* **59**, 12228.
 Cappelluti, E., C. Grimaldi, and F. Marsiglio, 2007, *Phys. Rev. B* **76**, 085334.
 Cho, J. H., and J. Y. Lee, 2007, *Phys. Rev. B* **76**, 033405.
 Cho, J. H., J. Y. Lee, and L. Kleinman, 2005, *Phys. Rev. B* **71**, 081310(R).
 Cho, J. H., D. H. Oh, K. S. Kim, and L. Kleinman, 2001, *Phys. Rev. B* **64**, 235302.
 Chuang, F.-C., C.-H. Hsu, C.-Z. Wang, and K.-M. Ho, 2008, *Phys. Rev. B* **77**, 153409.
 Crain, J. N., and F. J. Himpsel, 2006, *Appl. Phys. A: Mater. Sci. Process.* **82**, 431.
 Crain, J. N., A. Kirakosian, K. N. Altmann, C. Bromberger, S. C. Erwin, J. L. McChesney, J.-L. Lin, and F. J. Himpsel, 2003, *Phys. Rev. Lett.* **90**, 176805.
 Crain, J. N., J. L. McChesney, F. Zheng, M. C. Gallagher, P. C. Snijders, M. Bissen, C. Gundelach, S. C. Erwin, and F. J. Himpsel, 2004, *Phys. Rev. B* **69**, 125401.

- Crain, J. N., and D. T. Pierce, 2005, *Science* **307**, 703.
- Crain, J. N., M. D. Stiles, J. A. Stroschio, and D. T. Pierce, 2006, *Phys. Rev. Lett.* **96**, 156801.
- Erwin, S. C., 2003, *Phys. Rev. Lett.* **91**, 206101.
- Erwin, S. C., and H. H. Weitering, 1998, *Phys. Rev. Lett.* **81**, 2296.
- Gallus, O., T. Pillo, M. Hengsberger, P. Segovia, and Y. Baer, 2001, *Eur. Phys. J.: Appl. Phys.* **20**, 313.
- Ghose, S. K., I. K. Robinson, P. A. Bennett, and F. J. Himpsel, 2005, *Surf. Sci.* **581**, 199.
- González, C., F. Flores, and J. Ortega, 2006a, *Phys. Rev. Lett.* **97**, 189702.
- González, C., F. Flores, and J. Ortega, 2006b, *Phys. Rev. Lett.* **96**, 136101.
- González, C., J. D. Guo, J. Ortega, F. Flores, and H. H. Weitering, 2009, *Phys. Rev. Lett.* **102**, 115501.
- González, C., J. Ortega, and F. Flores, 2005, *New J. Phys.* **7**, 100.
- Grüner, G., 1988, *Rev. Mod. Phys.* **60**, 1129.
- Grüner, G., 1994, *Density Waves in Solids* (Perseus, Cambridge, MA).
- Grüner, G., and A. Zettl, 1985, *Phys. Rep.* **119**, 117.
- Guo, J., G. Lee, and E. W. Plummer, 2005, *Phys. Rev. Lett.* **95**, 046102.
- Gurlu, O., O. A. O. Adam, H. J. W. Zandvliet, and B. Poelsema, 2003, *Appl. Phys. Lett.* **83**, 4610.
- Hamers, R. J., R. M. Tromp, and J. E. Demuth, 1986, *Phys. Rev. B* **34**, 5343.
- Hill, I. G., and A. B. McLean, 1999, *Phys. Rev. B* **59**, 9791.
- Hwang, C. G., N. D. Kim, S. Y. Shin, and J. W. Chung, 2007, *New J. Phys.* **9**, 249.
- Jałochowski, M., M. Stróżak, and R. Zdyb, 1997, *Surf. Sci.* **375**, 203.
- Johannes, M. D., and I. I. Mazin, 2008, *Phys. Rev. B* **77**, 165135.
- Kim, K. S., H. Morikawa, W. H. Choi, and H. W. Yeom, 2007, *Phys. Rev. Lett.* **99**, 196804.
- Kirakosian, A., J. N. Crain, J.-L. Lin, J. L. McChesney, D. Y. Petrovykh, F. J. Himpsel, and R. Bennewitz, 2003, *Surf. Sci.* **532**, 928.
- Kraft, J., M. G. Ramsey, and F. P. Netzer, 1997, *Phys. Rev. B* **55**, 5384.
- Krawiec, M., T. Kwapiński, and M. Jałochowski, 2006, *Phys. Rev. B* **73**, 075415.
- Kumpf, C., O. Bunk, J. H. Zeysing, Y. Su, M. Nielsen, R. L. Johnson, R. Feidenhans'l, and K. Bechgaard, 2000, *Phys. Rev. Lett.* **85**, 4916.
- Kuper, C. G., 1955, *Proc. R. Soc. London, Ser. A* **227**, 214.
- Lander, J. J., and J. Morrison, 1965, *J. Appl. Phys.* **36**, 1706.
- LaShell, S., B. A. McDougall, and E. Jensen, 1996, *Phys. Rev. Lett.* **77**, 3419.
- Lee, G., 2006, *Surf. Interface Anal.* **38**, 1636.
- Lee, G., J. D. Guo, and E. W. Plummer, 2005, *Phys. Rev. Lett.* **95**, 116103.
- Lee, G., S.-Y. Yu, H. Kim, and J.-Y. Koo, 2004, *Phys. Rev. B* **70**, 121304(R).
- Lee, G., S. Y. Yu, H. Kim, J. Y. Koo, H. I. Lee, and D. W. Moon, 2003, *Phys. Rev. B* **67**, 035327.
- Lee, P. A., T. M. Rice, and P. W. Anderson, 1973, *Phys. Rev. Lett.* **31**, 462.
- Lipton-Duffin, J. A., J. M. MacLeod, and A. B. McLean, 2006, *Phys. Rev. B* **73**, 245418.
- Liu, C., T. Inaoka, S. Yaginuma, T. Nakayama, M. Aono, and T. Nagao, 2008, *Phys. Rev. B* **77**, 205415.
- López-Lozano, X., A. Krivosheeva, A. A. Stekolnikov, L. Meza-Montes, C. Noguez, J. Furthmüller, and F. Bechstedt, 2006, *Phys. Rev. B* **73**, 035430.
- Losio, R., K. N. Altmann, A. Kirakosian, J.-L. Lin, D. Y. Petrovykh, and F. J. Himpsel, 2001, *Phys. Rev. Lett.* **86**, 4632.
- Marin, F. P., and H. Suhl, 1989, *Phys. Rev. Lett.* **63**, 442.
- McChesney, J. L., J. N. Crain, V. Pérez-Dieste, F. Zheng, M. C. Gallagher, M. Bissen, C. Gundelach, and F. J. Himpsel, 2004, *Phys. Rev. B* **70**, 195430.
- McMillan, W. L., 1975, *Phys. Rev. B* **12**, 1187.
- Melechko, A. V., J. Braun, H. H. Weitering, and E. W. Plummer, 2000, *Phys. Rev. B* **61**, 2235.
- Mermin, N. D., and H. Wagner, 1966, *Phys. Rev. Lett.* **17**, 1133.
- Mizuno, S., Y. O. Mizuno, and H. Tochiyama, 2003, *Phys. Rev. B* **67**, 195410.
- Nagao, T., S. Yaginuma, T. Inaoka, and T. Sakurai, 2006, *Phys. Rev. Lett.* **97**, 116802.
- Nogami, J., S. I. Park, and C. F. Quate, 1987, *Phys. Rev. B* **36**, 6221.
- Nogami, J., S. I. Park, and C. F. Quate, 1988, *J. Vac. Sci. Technol. B* **6**, 1479.
- Okino, H., R. Hobara, I. Matsuda, T. Kanagawa, S. Hasegawa, J. Okabayashi, S. Toyoda, M. Oshima, and K. Ono, 2004, *Phys. Rev. B* **70**, 113404.
- Okino, H., I. Matsuda, S. Yamazaki, R. Hobara, and S. Hasegawa, 2007, *Phys. Rev. B* **76**, 035424.
- O'Mahony, J. D., J. F. McGilp, C. F. J. Flipse, P. Weightman, and F. M. Leibsle, 1994, *Phys. Rev. B* **49**, 2527.
- Oncel, N., A. van Houselt, J. Huijben, A. S. Hallböck, O. Gurlu, H. J. W. Zandvliet, and B. Poelsema, 2005, *Phys. Rev. Lett.* **95**, 116801.
- Park, S. J., H. W. Yeom, J. R. Ahn, and I.-W. Lyo, 2005, *Phys. Rev. Lett.* **95**, 126102.
- Park, S. J., H. W. Yeom, S. H. Min, D. H. Park, and I.-W. Lyo, 2004, *Phys. Rev. Lett.* **93**, 106402.
- Peierls, R. F., 1955, *Quantum Theory of Solids* (Clarendon, Oxford).
- Pérez, R., J. Ortega, and F. Flores, 2001, *Phys. Rev. Lett.* **86**, 4891.
- Psaltakis, G. S., 1985, *J. Phys. C* **18**, 2261.
- Ren, C.-Y., S.-F. Tsay, and F.-C. Chuang, 2007, *Phys. Rev. B* **76**, 075414.
- Riikonen, S., and D. Sánchez-Portal, 2005a, *Phys. Rev. B* **71**, 235423.
- Riikonen, S., and D. Sánchez-Portal, 2005b, *Nanotechnology* **16**, S218.
- Riikonen, S., and D. Sánchez-Portal, 2006, *Surf. Sci.* **600**, 1201.
- Riikonen, S., and D. Sánchez-Portal, 2007, *Phys. Rev. B* **76**, 035410.
- Riikonen, S., and D. Sánchez-Portal, 2008, *Phys. Rev. B* **77**, 165418.
- Robinson, I. K., P. A. Bennett, and F. J. Himpsel, 2002, *Phys. Rev. Lett.* **88**, 096104.
- Ryang, K.-D., P. G. Kang, H. W. Yeom, and S. Jeong, 2007, *Phys. Rev. B* **76**, 205325.
- Sakamoto, K., H. Ashima, H. W. Yeom, and W. Uchida, 2000, *Phys. Rev. B* **62**, 9923.
- Sánchez-Portal, D., S. Riikonen, and R. M. Martin, 2004, *Phys. Rev. Lett.* **93**, 146803.
- Sauter, M., R. Hoffmann, C. Sürgers, and H. v. Löhneysen, 2007, *Phys. Rev. B* **75**, 195436.
- Schäfer, J., C. Blumenstein, S. Meyer, M. Wisniewski, and R.

- Claessen, 2008, *Phys. Rev. Lett.* **101**, 236802.
- Schöck, M., C. Sürgers, and H. v. Löhneysen, 2003, *Thin Solid Films* **428**, 11.
- Schrieffer, J. R., 1973, *Nobel Symposium 24* (Academic, New York).
- Segovia, P., D. Purdie, M. Hengsberger, and Y. Baer, 1999, *Nature (London)* **402**, 504.
- Snijders, P. C., 2006, Ph.D. thesis (Delft University of Technology).
- Snijders, P. C., S. Rogge, C. Gonzalez, R. Perez, J. Ortega, F. Flores, and H. H. Weitering, 2005, *Phys. Rev. B* **72**, 125343.
- Snijders, P. C., S. Rogge, and H. H. Weitering, 2006, *Phys. Rev. Lett.* **96**, 076801.
- Starowicz, P., O. Gallus, T. Pillo, and Y. Baer, 2002, *Phys. Rev. Lett.* **89**, 256402.
- Stekolnikov, A. A., K. Seino, F. Bechstedt, S. Wippermann, W. G. Schmidt, A. Calzolari, and M. Buongiorno Nardelli, 2007, *Phys. Rev. Lett.* **98**, 026105.
- Stevens, J. L., M. S. Worthington, and I. S. T. Tsong, 1993, *Phys. Rev. B* **47**, 1453.
- Sun, Y. J., S. Agario, S. Souma, K. Sugawara, Y. Tago, T. Sato, and T. Takahashi, 2008, *Phys. Rev. B* **77**, 125115.
- Tanikawa, T., I. Matsuda, T. Kanagawa, and S. Hasegawa, 2004, *Phys. Rev. Lett.* **93**, 016801.
- Tegenkamp, C., Z. Kallassy, H. Pfnür, H.-L. Günter, V. Zielasek, and M. Henzler, 2005, *Phys. Rev. Lett.* **95**, 176804.
- Tegenkamp, C., T. Ohta, J. L. McChesney, H. Dil, E. Rotenberg, H. Pfnür, and K. Horn, 2008, *Phys. Rev. Lett.* **100**, 076802.
- Tsay, S. F., 2005, *Phys. Rev. B* **71**, 035207.
- Uchihashi, T., and U. Ramsperger, 2002, *Appl. Phys. Lett.* **80**, 4169.
- Voit, J., 1995, *Rep. Prog. Phys.* **58**, 977.
- Wang, J., H. S. Wu, R. So, Y. Liu, M. H. Xie, and S. Y. Tong, 2005, *Phys. Rev. B* **72**, 245324.
- Wang, S. C., W. C. Lu, W. G. Schmidt, and J. Bernholc, 2003, *Phys. Rev. B* **68**, 035329.
- Weitering, H. H., J. M. Carpinelli, A. V. Melechko, J. Zhang, M. Bartkowiak, and E. W. Plummer, 1999, *Science* **285**, 5436.
- Wiekliem, P. C., G. W. Smith, and E. A. Carter, 1990, *Surf. Sci.* **232**, L219.
- Yagi, Y., H. Kaji, K. Kakitani, and S. Osanaga, 2008, *C. R. Acad. Sci. URSS, Ser. A* **100**, 072039.
- Yagi, Y., and A. Yoshimori, 2005, *J. Phys. Soc. Jpn.* **74**, 831.
- Yagi, Y., A. Yoshimori, K. Kakitani, and H. Kaji, 2007, *Surf. Sci.* **601**, 1642.
- Yeom, H. W., 2006, *Phys. Rev. Lett.* **97**, 189701.
- Yeom, H. W., J. R. Ahn, H. S. Yoon, I.-W. Lyo, H. Jeong, and S. Jeong, 2005, *Phys. Rev. B* **72**, 035323.
- Yeom, H. W., K. Horikoshi, H. M. Zhang, K. Ono, and R. I. G. Uhrberg, 2002, *Phys. Rev. B* **65**, 241307(R).
- Yeom, H. W., S. Takeda, E. Rotenberg, I. Matsuda, K. Horikoshi, J. Schaefer, C. M. Lee, S. D. Kevan, T. Ohta, T. Nagao, and S. Hasegawa, 1999, *Phys. Rev. Lett.* **82**, 4898.
- Yoon, H. S., J. E. Lee, S. J. Park, I.-W. Lyo, and M.-H. Kang, 2005, *Phys. Rev. B* **72**, 155443.
- Yoon, H. S., S. J. Park, J. E. Lee, C. N. Whang, and I.-W. Lyo, 2004, *Phys. Rev. Lett.* **92**, 096801.